

RESEARCH PAPER



# Synthesis, molecular modelling and QSAR study of new *N*-phenylacetamide-2-oxindole benzenesulfonamide conjugates as carbonic anhydrase inhibitors with antiproliferative activity

Mona F. Said<sup>a</sup>, Riham F. George<sup>a</sup> , Andrea Petreni<sup>b</sup>, Claudiu T. Supuran<sup>b</sup>  and Nada M. Mohamed<sup>c</sup>

<sup>a</sup>Department of Pharmaceutical Chemistry, Faculty of Pharmacy, Cairo University, Cairo, Egypt; <sup>b</sup>Department of NEUROFARBA, Section of Pharmaceutical and Nutraceutical Sciences, University of Florence, Florence, Italy; <sup>c</sup>Department of Pharmaceutical Chemistry, Faculty of Pharmacy, Modern University for Technology and Information MTI, Cairo, Egypt

## ABSTRACT

In continuation of our previous studies to optimise potent carbonic anhydrase inhibitors, two new series of isatin *N*-phenylacetamide based sulphonamides were synthesised and screened for their human (h) carbonic anhydrase (EC 4.2.1.1) inhibitory activities against four isoforms *hCA* I, *hCA* II, *hCA* IX and *hCA* XII. The indole-2,3-dione derivative **2h** showed the most effective inhibition profile against *hCA*I and *hCA* II ( $K_i = 45.10, 5.87$  nM) compared to acetazolamide (**AAZ**) as standard inhibitor. Moreover, **2h** showed appreciable inhibition activity against the tumour-associated *hCA* XII, similar to **AAZ** showing  $K_i$  of 7.91 and 5.70 nM, respectively. The analogs **3c** and **3d** showed good cytotoxicity effects, and **3c** revealed promising selectivity towards lung cell line A549. Molecular docking was carried out for **2h** and **3c** to predict their binding conformations and affinities towards the *hCA* I, II, IX and XII isoforms.

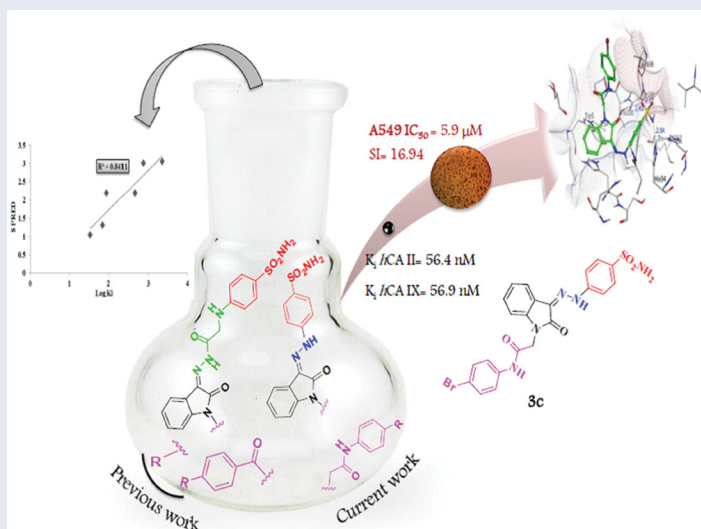
## ARTICLE HISTORY

Received 22 December 2021  
Revised 24 January 2022  
Accepted 25 January 2022

## KEYWORDS

Carbonic anhydrase inhibitors; benzenesulfonamides; molecular docking; 2D-QSAR study

## GRAPHICAL ABSTRACT








## 1. Introduction

The simple and fundamental interconversion of crucial ion species such as carbon dioxide and bicarbonate ( $CO_2/HCO_3^-$ ) occurs during biochemical processes in all living organisms. The  $CO_2/HCO_3^-$  interconversion is catalysed by a superfamily of metalloenzymes called carbonic anhydrases (CAs, EC 4.2.1.1). The enzymes belonging to the  $\alpha$ -CA family tightly coordinate a  $Zn^{2+}$  ion within their active sites, that interacts with a water molecule and histidine

residues in a tetrahedral geometry of the metal ion. The zinc ion binds and activates a water molecule to catalyse the hydration reaction of carbon dioxide to bicarbonate and proton ions by a metal hydroxide nucleophilic mechanism. Consequently, CAs act among the major physiological buffering systems<sup>1–4</sup>.

Human CAs (*hCAs*) are represented by 15 isoforms which include the cytosolic (I, II, III, VII, XIII), mitochondrial (VA, VB), secreted (VI), and membrane associated (IV, IX, XII, XIV) in addition

**CONTACT** Riham F. George  [riham.eskandar@pharma.cu.edu.eg](mailto:riham.eskandar@pharma.cu.edu.eg)  Department of Pharmaceutical Chemistry, Faculty of Pharmacy, Cairo University, Cairo, Egypt; Claudiu T. Supuran  [claudiu.supuran@unifi.it](mailto:claudiu.supuran@unifi.it)  Department of NEUROFARBA, Section of Pharmaceutical and Nutraceutical Sciences, University of Florence, Florence, Italy

 Supplemental data for this article can be accessed [here](#).

© 2022 The Author(s). Published by Informa UK Limited, trading as Taylor & Francis Group.

This is an Open Access article distributed under the terms of the Creative Commons Attribution-NonCommercial License (<http://creativecommons.org/licenses/by-nc/4.0/>), which permits unrestricted non-commercial use, distribution, and reproduction in any medium, provided the original work is properly cited.

to the catalytic isoforms of carbonic anhydrase related proteins located in cytosol (VIII, X, XI)<sup>5-8</sup>. Fluctuation in CA expression levels can lead to hypertension, glaucoma, epilepsy, neuropathic pain, cancer, etc. Accordingly, many *hCA* isoforms are considered as attractive therapeutic targets for many pharmacological applications<sup>9,10</sup>. Recently, CA inhibitors (CAIs) were adopted as a combination therapy for solid tumours upon acknowledging the overexpression of the membrane-associated isoenzymes *hCA IX* and *hCA XII* in that kind of tumours. Those isoenzymes were discovered to play pivotal role in microenvironment pH regulation thus being important in the survival, proliferation, metastasis and development of drug resistance of malignant cells<sup>11,12</sup>.

Known CAIs are generally primary aromatic or heteroaromatic sulphonamides in which the sulphonamide moiety coordinates the  $Zn^{+2}$  ion in the enzyme active site with their terminal deprotonated nitrogen atom simulating the known non-selective CAI Acetazolamide (AAZ) **I** (Figure 1)<sup>13-15</sup>. Sulphonamide based CAIs

have versatile pharmacological activities such as diuretic<sup>16</sup>, anti-glaucoma<sup>17</sup>, antiepileptic<sup>18</sup>, antimicrobial<sup>19</sup>, anti-inflammatory<sup>20</sup>, antioxidant<sup>21</sup> and anticancer<sup>22-24</sup>. These activities made them attractive candidates for developing novel agents with varying biological activities through minor structural alterations<sup>9,10</sup>.

Moreover, isatin (indole-2,3-dione) is considered as a crucial core in many anticancer drugs in the market as sunitinib **II**<sup>25</sup>. Furthermore, isatin-benzenesulfonamide conjugates were reported to have promising anticancer activity as well as carbonic anhydrase inhibition<sup>26-28</sup>. For example, 4-(2-(1-ethyl-2-oxindolin-3-ylidene)hydrazine-1-carbonyl)benzenesulfonamide (**III**) revealed  $K_i = 8.9$  nM against *hCA IX*<sup>26</sup>. Additionally, isatin hydrazinyl benzenesulfonamide derivative **IV** exhibited  $K_i = 7.8$  nM against *hCA IX* isoform<sup>27</sup>. Based on this knowledge, the present study was designed to develop potent and selective isatin-based sulphonamide CAIs utilising the "tail approach". This approach investigated the effect of adding different molecular fragments to the isatin scaffold on

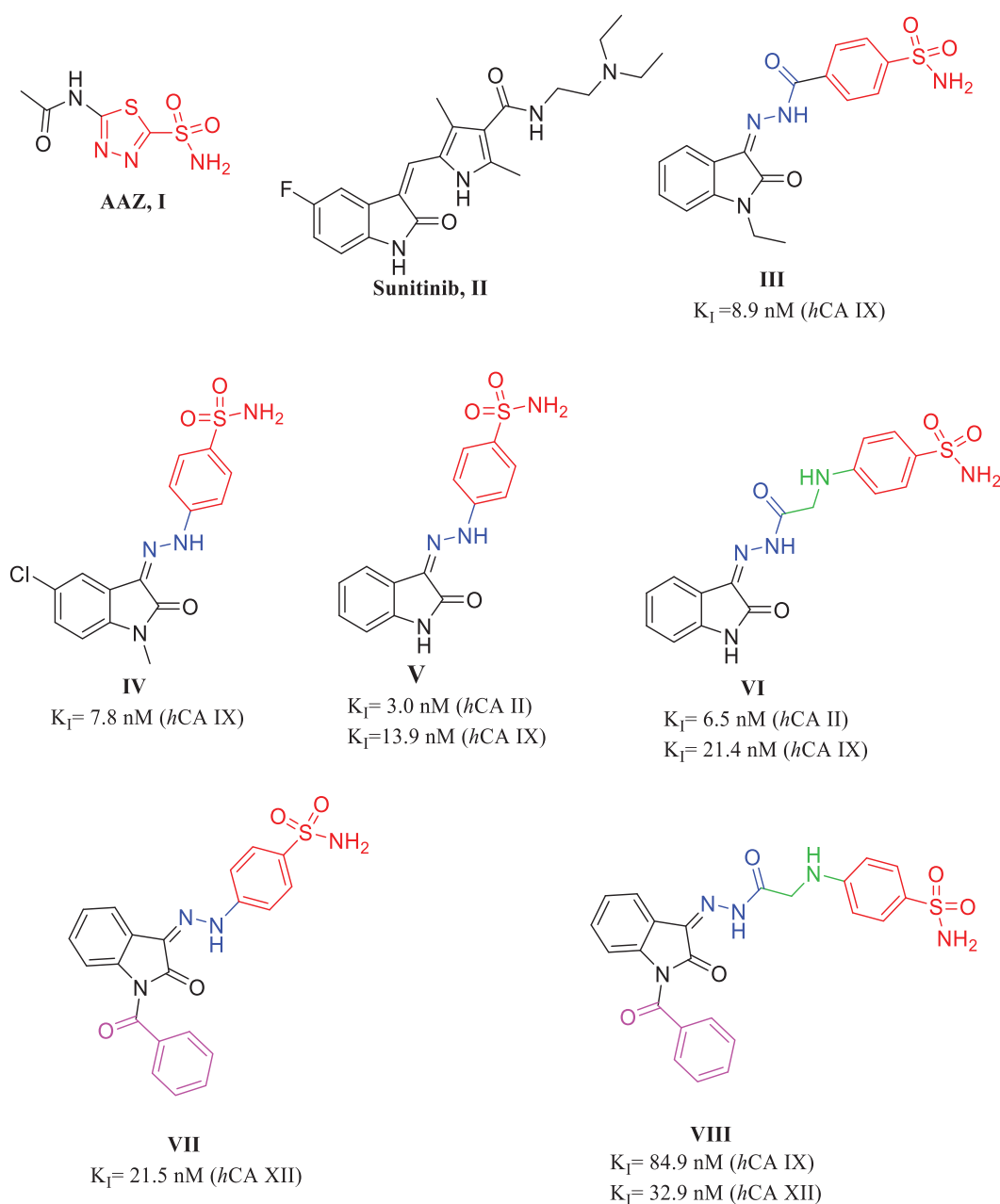


**Figure 1.** Chemical structures of AAZ (**I**), Sunitinib (**II**) and reported CAIs incorporating sulphonamide moieties **III-VIII**.

the binding interaction with the enzyme active site which in turn would modulate the potency and selectivity<sup>29,30</sup>.

Previously reported unsubstituted isatin Schiff's bases **V** and **VI** showed promising CA inhibitory activity<sup>29</sup> (Figure 1), then the developed *N*-benzoyl candidates showed high potency and selectivity towards *h*CA XII (compounds **VII**, **VIII**)<sup>30</sup> (Figure 1). Motivated by these results, we developed here new isatin-based sulphonamide candidates by incorporation of phenylacetamide moiety at the isatin nitrogen as a new structural modification. The attached phenylacetamide moiety was evaluated as unsubstituted as well as substituted by groups of diverse size, lipophilicity, and electronic property (such as Cl, Br, CH<sub>3</sub>, OCH<sub>3</sub>, SO<sub>2</sub>NH<sub>2</sub>) to investigate the interaction of the new adopted tail fragment with the CA active site. Additionally, the isatin scaffold was hybridised with the benzene sulphonamide through a hydrazinyl (compounds **3a-g**), or hydrazinyl-2-oxoethylamino spacers (compounds **4a-g**) in order to study the effect of this structure elongation along with the tail fragment on the CA inhibitory activity and selectivity (Figure 2). All new synthesised candidates (**2h**, **3a-g**, **4a-g**) were screened for their CA inhibitory activity against four *h*CA isoforms (I, II, IX, and XII), and the most active ones were selected for further *in vitro* evaluation for their anti-proliferative activity. Furthermore, to rationalise their significant *in vitro* biological results, molecular docking simulation was carried out for the most active derivatives to study their binding pattern and affinity to the *h*CA II, IV, IX, and XII active sites. Furthermore, 2D-QSAR study was performed using all reported derivatives of our previous work<sup>29,30</sup> in addition to

the newly synthesised derivatives to obtain two validated models for the tumour associated isoforms *h*CA IX and XII elucidating the descriptors controlling the activity, therefore they can be used for prediction of activity of further isatin-based derivatives.

## 2. Experimental

### 2.1. Chemistry

All chemicals were purchased from VWR International Merck, or Sigma-Aldrich, Germany. Melting points are uncorrected and were measured by open capillary tube method using Stuart SMP3 melting point apparatus. Elemental microanalyses were carried out at the Regional Centre for Mycology and Biotechnology, Al-Azhar University. Infra-red spectra were recorded on Shimadzu spectrometer IR Affinity-1 (FTIR- 8400S-Kyoto-Japan) and expressed in wave number (cm<sup>-1</sup>). <sup>1</sup>H NMR and <sup>13</sup>C NMR Spectra were recorded on Bruker High Performance Digital FT-NMR Spectrometer Avance III 400 MHz, <sup>13</sup>C, 100 MHz NMR spectrometer. Chemical shifts were expressed in δ units and were related to that of the solvents. Mass Spectra were recorded using ISQLT Thermo Scientific Mass spectrometer at The Regional Centre for Mycology and Biotechnology, Al-Azhar University. All the reactions were monitored by TLC using silica gel F254 plates (Sigma-Aldrich), using chloroform: methanol 9.5:0.5 as eluting system and were visualised by UV-lamp. Compounds **1a-g**<sup>31,32</sup>, **2a-f**<sup>33-35</sup>, and the reagents 4-hydrazinylbenzenesulfonamide hydrochloride<sup>36</sup> and 4-

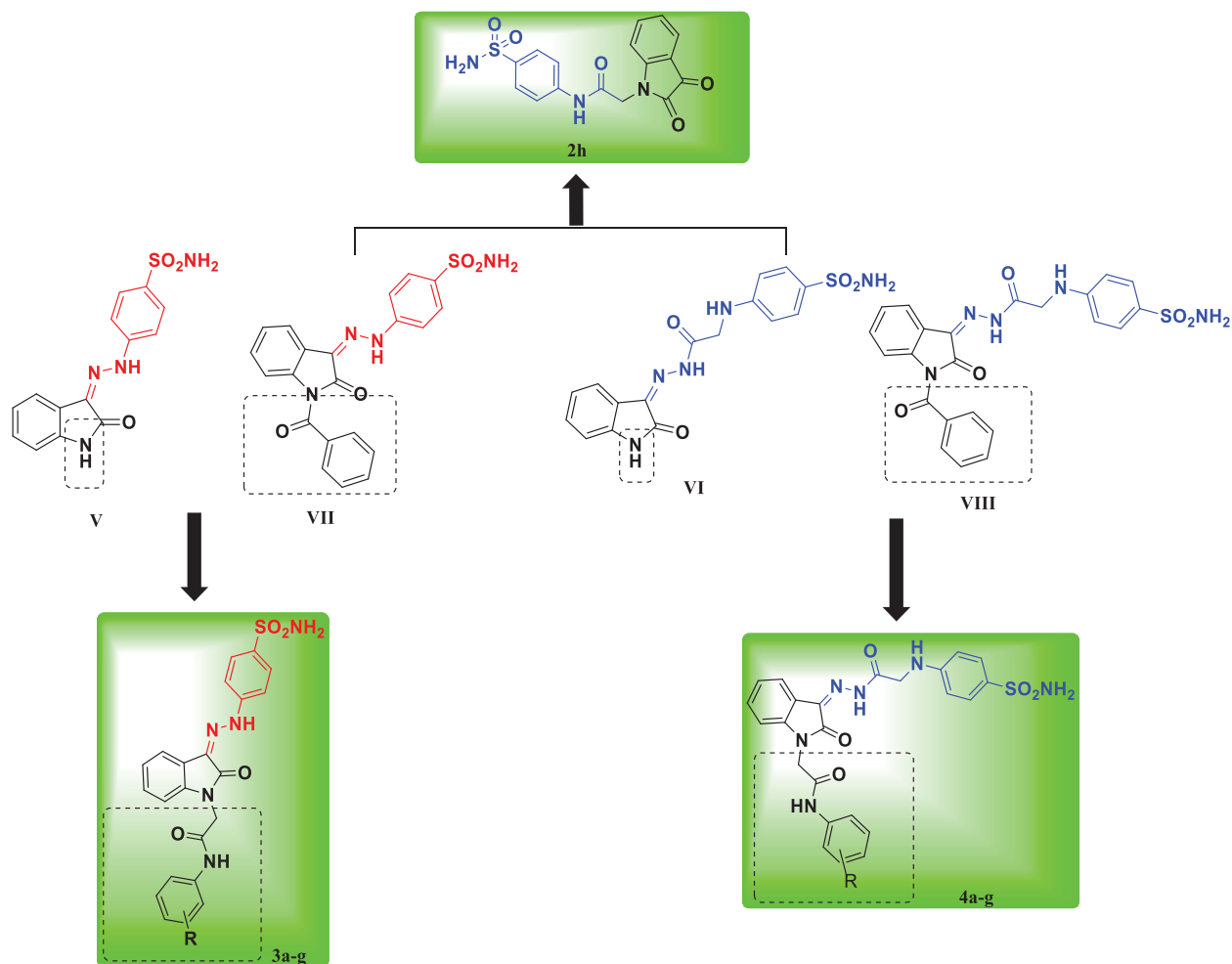


Figure 2. The rationale of the newly synthesised isatin-based sulphonamide derivatives **2h**, **3a-g** and **4a-g**.

(2-hydrazinyl-2-oxoethylamino)benzenesulfonamide<sup>37</sup> were prepared according to their reported methods.

### 2.1.1. General procedure for the synthesis of compounds 2a-h

A mixture of isatin (indole-2,3-dione) (0.29 g, 2 mmol) and potassium carbonate (0.82 g, 6 mmol) was stirred for 15 min. in DMF (5 ml), then an appropriate 2-chloro-*N*-phenylacetamide (**1a-h**) (2 mmol) was added. The reaction was stirred at room temperature for 4 h, then poured on ice water, the precipitated solid was filtered, washed with water and crystallised from methanol.

#### 2.1.1.1. *N*-(2-Bromophenyl)-2-(2,3-dioxindolin-1-yl)acetamide (2g)

Yellow crystals, yield 80%, m.p. 221–222 °C; IR (KBr,  $\nu$  cm<sup>-1</sup>): 3244 (NH), 3036 (CH aromatic), 2931 (CH aliphatic), 1736, 1670 (3 C=O), 1612 (NH bending), 1589, 1531 (C=C); <sup>1</sup>H NMR (CDCl<sub>3</sub>, 400 MHz):  $\delta$  4.62 (s, 2H, NCH<sub>2</sub>), 7.17–7.20 (m, 3H, aromatic H), 7.38 (t, 1H,  $J$  = 7.64 Hz, aromatic H), 7.50 (d,  $J$  = 7.04 Hz, 1H, aromatic H), 7.63 (d,  $J$  = 6.60 Hz, 1H, aromatic H), 7.66–7.73 (m, 2H, aromatic H), 9.94 (s, 1H, NH, D<sub>2</sub>O exchangeable); <sup>13</sup>C NMR (CDCl<sub>3</sub>, 100 MHz):  $\delta$  44.7 (CH<sub>2</sub>), 110.8, 117.8, 122.1, 124.7, 125.8, 126.1, 128.5, 132.4, 134.6, 138.8, 149.9 (aromatic carbons), 158.3, 163.8, 181.9 (3 C=O); MS,  $m/z$  [%]: 361.10 [M<sup>+</sup>+2, 3.27], 359.10 [M<sup>+</sup>, 3.87]; Anal. Calcd. for C<sub>16</sub>H<sub>11</sub>BrN<sub>2</sub>O<sub>3</sub> (359.17): C, 53.50; H, 3.09; N, 7.80. Found: C, 53.74; H, 3.25; N, 8.07.

#### 2.1.1.2. 2-(2,3-Dioxindolin-1-yl)-*N*-(4-sulfamoylphenyl)acetamide (2h)

Yellow orange crystals, yield 78%, m.p. 237–238 °C; IR (KBr,  $\nu$  cm<sup>-1</sup>): 3325, 3267, 3205 (NH<sub>2</sub>, NH), 3067 (CH aromatic), 2935 (CH aliphatic), 1740, 1697 (3 C=O), 1612 (NH bending), 1597, 1543 (C=C), 1308, 1153 (SO<sub>2</sub>); <sup>1</sup>H NMR (DMSO-d<sub>6</sub>, 400 MHz):  $\delta$  4.63 (s, 2H, NCH<sub>2</sub>), 7.16–7.18 (m, 2H, aromatic H), 7.28 (s, 2H, NH<sub>2</sub>, D<sub>2</sub>O exchangeable), 7.62–7.73 (m, 4H, aromatic H), 7.78 (d,  $J$  = 8.64 Hz, 2H, aromatic H), 10.59 (s, 1H, NH, D<sub>2</sub>O exchangeable); <sup>13</sup>C NMR (DMSO-d<sub>6</sub>, 100 MHz):  $\delta$  43.7 (CH<sub>2</sub>), 111.5, 118.0, 119.6, 124.0, 125.0, 127.2, 138.8, 139.4, 141.7, 151.3 (aromatic carbons), 158.9, 166.0, 183.4 (C=O); MS,  $m/z$  [%]: 360.15 [M<sup>+</sup>+1, 5.37], 359.20 [M<sup>+</sup>, 22.48]; Anal. Calcd. for C<sub>16</sub>H<sub>13</sub>N<sub>3</sub>O<sub>5</sub>S (359.36): C, 53.48; H, 3.65; N, 11.69. Found: C, 53.69; H, 3.80; N, 11.88.

### 2.1.2. General procedure for the synthesis of compounds 3a-g

A mixture of equimolar amounts of (**2a-g**) (1 mmol) and 4-hydrazinylbenzenesulfonamide hydrochloride (0.22 g, 1 mmol) in methanol (5 ml) was stirred at room temperature for 4 h. The obtained solid was filtered, washed with ethanol and recrystallized from ethanol.

#### 2.1.2.1. 2-(2-Oxo-3-(2-(4-sulfamoylphenyl)hydrazono)indolin-1-yl)-*N*-phenylacetamide (3a)

Yellow crystals, yield 78%, m.p. 294–295 °C; IR (KBr,  $\nu$  cm<sup>-1</sup>): 3364, 3329 (NH<sub>2</sub>), 3197, 3140 (2NH), 3059 (CH aromatic), 2974 (CH aliphatic), 1700, 1678 (2 C=O), 1605 (NH bending), 1570, 1551 (C=C), 1300, 1157 (SO<sub>2</sub>); <sup>1</sup>H NMR (DMSO-d<sub>6</sub>, 400 MHz):  $\delta$  4.65, 4.70 (2 s, 2H, NCH<sub>2</sub>), 7.05–7.10, 7.13–7.19 (2 m, 3H, aromatic H), 7.25, 7.27 (2 s, 2H, NH<sub>2</sub>, D<sub>2</sub>O exchangeable), 7.31–7.36, 7.37–7.43 (2 m, 4H, aromatic H), 7.59, 7.68 (2d,  $J$  = 7.72 Hz, 2H, aromatic H), 7.62, 7.68 (2d,  $J$  = 7.72 Hz, 2H, aromatic H), 7.82, 7.84 (2d,  $J$  = 7.30 Hz, 2H, aromatic H), 10.34, 10.38 (2 s, 1H, NH, D<sub>2</sub>O exchangeable), 10.86, 12.68 (2 s, 1H, NH, D<sub>2</sub>O exchangeable); <sup>13</sup>C NMR (DMSO-d<sub>6</sub>, 100 MHz):  $\delta$  43.1 (NCH<sub>2</sub>), 109.7, 114.5, 115.1, 119.4, 122.3, 123.1, 124.1, 127.6, 129.3, 129.7, 138.3, 139.0, 141.9, 145.6 (aromatic carbons), 161.7, 165.5 (C=O);

MS,  $m/z$  [%]: 449 [M<sup>+</sup>, 40]; Anal. Calcd. for C<sub>22</sub>H<sub>19</sub>N<sub>5</sub>O<sub>4</sub>S (449.48): C, 58.79; H, 4.26; N, 15.58. Found: C, 59.03; H, 4.42; N, 15.79.

#### 2.1.2.2. *N*-(4-Chlorophenyl)-2-(2-oxo-3-(2-(4-sulfamoylphenyl)hydrazono)indolin-1-yl)acetamide (3b)

Yellow crystals, yield 75%, m.p. 297–298 °C; IR (KBr,  $\nu$  cm<sup>-1</sup>): 3282 (NH<sub>2</sub>, 2 NH), 3067 (CH aromatic), 2932 (CH aliphatic), 1693, 1674 (2 C=O), 1601 (NH bending), 1570, 1539 (C=C), 1331, 1153 (SO<sub>2</sub>); <sup>1</sup>H NMR (DMSO-d<sub>6</sub>, 400 MHz):  $\delta$  4.65, 4.70 (2 s, 2H, NCH<sub>2</sub>), 7.09–7.14, 7.16–7.20 (2 m, 4H, aromatic H), 7.24, 7.26 (2 s, 2H, NH<sub>2</sub>, D<sub>2</sub>O exchangeable), 7.61–7.64, 7.66–7.69 (2 m, 4H, aromatic H), 7.81–7.85 (m, 3H, aromatic H), 8.31 (d,  $J$  = 7.68 Hz, 1H, aromatic H), 10.49, 10.86 (2 s, 1H, NH, D<sub>2</sub>O exchangeable), 10.52, 12.67 (2 s, 1H, NH, D<sub>2</sub>O exchangeable); <sup>13</sup>C NMR (DMSO-d<sub>6</sub>, 100 MHz):  $\delta$  43.0, 43.3 (NCH<sub>2</sub>), 109.7, 110.1, 114.5, 115.1, 116.0, 119.5, 120.6, 121.2, 121.3, 122.4, 123.2, 124.8, 127.6, 127.7, 128.0, 129.1, 129.2, 129.7, 131.1, 137.9, 138.0, 138.3, 141.8, 143.3, 145.6, 147.2 (aromatic carbons), 161.7, 164.7, 165.8, 166.0 (2 C=O); MS,  $m/z$  [%]: 486.15 [M<sup>+</sup>+2, 13], 484.17 [M<sup>+</sup>+1, 24]; Anal. Calcd. for C<sub>22</sub>H<sub>18</sub>ClN<sub>5</sub>O<sub>4</sub>S (483.93): C, 54.60; H, 3.75; N, 16.85. Found: C, 54.87; H, 3.92; N, 14.68.

#### 2.1.2.3. *N*-(4-Bromophenyl)-2-(2-oxo-3-(2-(4-sulfamoylphenyl)hydrazono)indolin-1-yl)acetamide (3c)

Yellow crystals, yield 75%, m.p. 300–302 °C; IR (KBr,  $\nu$  cm<sup>-1</sup>): 3333, 3267, 3155 (NH<sub>2</sub>, 2NH), 3059 (CH aromatic), 2931 (CH aliphatic), 1712, 1674 (2 C=O), 1605 (NH bending), 1570, 1539 (C=C), 1296, 1157 (SO<sub>2</sub>); <sup>1</sup>H NMR (DMSO-d<sub>6</sub>, 400 MHz):  $\delta$  4.65, 4.70 (2 s, 2H, NCH<sub>2</sub>), 7.10 (d,  $J$  = 7.92 Hz, 1H, aromatic H), 7.15 (t,  $J$  = 7.34 Hz, 1H, aromatic H), 7.25 (s, 2H, NH<sub>2</sub>, D<sub>2</sub>O exchangeable), 7.40 (t,  $J$  = 7.68 Hz, 1H, aromatic H), 7.50 (d,  $J$  = 8.92 Hz, 2H, aromatic H), 7.56 (d,  $J$  = 8.92 Hz, 2H, aromatic H), 7.65 (d,  $J$  = 8.84 Hz, 2H, aromatic H), 7.84 (d,  $J$  = 8.72 Hz, 2H, aromatic H), 8.30 (d, 1H,  $J$  = 7.64 Hz, aromatic H), 10.49, 10.53 (2 s, 1H, NH, D<sub>2</sub>O exchangeable), 10.87, 12.67 (2 s, 1H, NH, D<sub>2</sub>O exchangeable); <sup>13</sup>C NMR (DMSO-d<sub>6</sub>, 100 MHz):  $\delta$  43.14, 43.33 (NCH<sub>2</sub>), 109.7, 110.1, 114.5, 115.1, 115.6, 115.7, 116.0, 119.5, 120.6, 121.6, 121.7, 122.4, 123.1, 124.8, 127.7, 127.9, 129.1, 129.7, 131.2, 138.04, 138.3, 141.8, 143.3, 145.6, 147.2 (aromatic carbons), 161.7, 164.6, 165.8, 166.1 (2 C=O); MS,  $m/z$  [%]: 528.02 [M<sup>+</sup>, 25]; Anal. Calcd. for C<sub>22</sub>H<sub>18</sub>BrN<sub>5</sub>O<sub>4</sub>S (528.38): C, 50.01; H, 3.43; N, 13.25. Found: C, 50.12; H, 3.67; N, 13.49.

#### 2.1.2.4. 2-(2-Oxo-3-(2-(4-sulfamoylphenyl)hydrazono)indolin-1-yl)-*N*-*p*-tolylacetamide (3d)

Yellow crystals, yield 73%, m.p. 298–299 °C; IR (KBr,  $\nu$  cm<sup>-1</sup>): 3341, 3171 (NH<sub>2</sub>, 2NH), 3059 (CH aromatic), 2939 (CH aliphatic), 1713, 1682 (2 C=O), 1605 (NH bending), 1570, 1547 (C=C), 1296, 1157 (SO<sub>2</sub>); <sup>1</sup>H NMR (DMSO-d<sub>6</sub>, 400 MHz):  $\delta$  2.26 (s, 3H, CH<sub>3</sub>), 4.63, 4.68 (2 s, 2H, NCH<sub>2</sub>), 7.09–7.19 (m,  $J$  = 8.08 Hz, 4H, aromatic H), 7.25, 7.27 (2 s, 2H, NH<sub>2</sub>, D<sub>2</sub>O exchangeable), 7.41 (t,  $J$  = 7.74 Hz, 1H, aromatic H), 7.47 (d,  $J$  = 8.28 Hz, 2H, aromatic H), 7.66 (d, 2H,  $J$  = 8.72 Hz, aromatic H), 7.84 (d,  $J$  = 8.60 Hz, 2H, aromatic H), 8.31 (d,  $J$  = 7.64 Hz, 1H, aromatic H), 10.27, 10.31 (2 s, 1H, NH, D<sub>2</sub>O exchangeable), 10.87, 12.68 (2 s, 1H, NH, D<sub>2</sub>O exchangeable); <sup>13</sup>C NMR (DMSO-d<sub>6</sub>, 100 MHz):  $\delta$  20.9 (CH<sub>3</sub>), 43.0, 43.2 (NCH<sub>2</sub>), 109.7, 110.3, 114.4, 115.1, 116.0, 119.4, 119.6, 119.7, 120.5, 122.3, 123.1, 124.8, 127.6, 127.8, 129.1, 129.6, 131.1, 131.2, 132.9, 133.0, 136.5, 136.6, 138.0, 138.3, 141.9, 143.4, 145.6, 147.1 (aromatic H), 161.7, 164.6, 165.2, 165.6 (C=O); MS,  $m/z$  [%]: 463.51 [M<sup>+</sup>, 39]; Anal. Calcd. for C<sub>23</sub>H<sub>21</sub>N<sub>5</sub>O<sub>4</sub>S (463.51): C, 59.60; H, 4.57; N, 15.11. Found: C, 59.84; H, 4.73; N, 15.38.

**2.1.2.5. *N*-(4-Methoxyphenyl)-2-(2-oxo-3-(2-(4-sulfamoylphenyl)hydrazono)indolin-1-yl) acetamide (3e).** Yellow crystals, yield 70%, m.p. 294–295 °C; IR (KBr,  $\nu$   $\text{cm}^{-1}$ ): 3333, 3213, 3171 ( $\text{NH}_2$ , 2NH), 3040 (CH aromatic), 2978, 2935 (CH aliphatic), 1713, 1678 (2 C=O), 1609 (NH bending), 1570, 1547 (C=C), 1300, 1157 ( $\text{SO}_2$ );  $^1\text{H}$  NMR (DMSO- $d_6$ , 400 MHz):  $\delta$  3.72 (s, 3H,  $\text{OCH}_3$ ), 4.61, 4.62 (2s, 2H,  $\text{NCH}_2$ ), 6.89 (d,  $J$  = 8.88 Hz, 2H, aromatic H), 7.09 (d,  $J$  = 7.88 Hz, 1H, aromatic H), 7.17 (t,  $J$  = 7.58 Hz, 1H, aromatic H), 7.25, 7.27 (2s, 2H,  $\text{NH}_2$ ,  $\text{D}_2\text{O}$  exchangeable), 7.41 (t,  $J$  = 7.74 Hz, 1H, aromatic H), 7.49 (d,  $J$  = 8.88 Hz, 2H, aromatic H), 7.65 (d,  $J$  = 8.80 Hz, 2H, aromatic H), 7.84 (d,  $J$  = 8.64 Hz, 2H, aromatic H), 8.30 (d,  $J$  = 7.64 Hz, 1H, aromatic H), 10.20, 10.21 (2s, 1H, NH,  $\text{D}_2\text{O}$  exchangeable), 10.86, 12.69 (2s, 1H, NH,  $\text{D}_2\text{O}$  exchangeable);  $^{13}\text{C}$  NMR (DMSO- $d_6$ , 100 MHz):  $\delta$  43.0, 43.2 ( $\text{NCH}_2$ ), 55.6 ( $\text{OCH}_3$ ), 109.7, 110.1, 114.4, 114.5, 115.1, 116.0, 119.5, 120.6, 121.2, 121.3, 122.4, 123.1, 124.8, 127.7, 127.9, 129.2, 129.7, 131.1, 131.3, 132.1, 132.2, 138.0, 138.3, 141.9, 143.4, 145.6, 147.2, 155.8, 155.9 (aromatic carbons), 161.7, 164.6, 165.0, 165.3 (C=O); MS,  $m/z$  [%]: 479.47 [ $\text{M}^+$ , 26]; Anal. Calcd. for  $\text{C}_{23}\text{H}_{21}\text{N}_5\text{O}_5\text{S}$  (479.51): C, 57.61; H, 4.41; N, 14.61. Found: C, 57.49; H, 4.63; N, 14.88.

**2.1.2.6. *N*-(2-Chlorophenyl)-2-(2-oxo-3-(2-(4-sulfamoylphenyl)hydrazono)indolin-1-yl) acetamide (3f).** Yellow crystals, yield 78%, m.p. 275–276 °C; IR (KBr,  $\nu$   $\text{cm}^{-1}$ ): 3363, 3333, 3136 ( $\text{NH}_2$ , 2NH), 3059 (CH aromatic), 2974, 2935 (CH aliphatic), 1701 (2 C=O), 1601 (NH bending), 1570, 1512 (C=C), 1296, 1153 ( $\text{SO}_2$ );  $^1\text{H}$  NMR (DMSO- $d_6$ , 400 MHz):  $\delta$  4.73, 4.78 (2s, 2H,  $\text{NCH}_2$ ), 6.93 (d,  $J$  = 7.20 Hz, 1H, aromatic H), 7.13–7.23 (m, 2H, aromatic H), 7.27 (s, 2H,  $\text{NH}_2$ ,  $\text{D}_2\text{O}$  exchangeable), 7.30–7.41 (m, 2H, aromatic H), 7.51 (d,  $J$  = 8.40 Hz, 1H, aromatic H), 7.62 (d,  $J$  = 8.80 Hz, 2H, aromatic H), 7.68 (t,  $J$  = 8.40 Hz, 1H, aromatic H), 7.82 (d,  $J$  = 8.80 Hz, 2H, aromatic H), 8.30 (d,  $J$  = 8.00 Hz, 1H, aromatic H), 9.99, 11.10 (2s, 1H, NH,  $\text{D}_2\text{O}$  exchangeable), 12.66 (s, 1H, NH,  $\text{D}_2\text{O}$  exchangeable);  $^{13}\text{C}$  NMR (DMSO- $d_6$ , 100 MHz):  $\delta$  42.8 ( $\text{NCH}_2$ ), 110.1, 114.2, 114.4, 119.4, 120.6, 123.1, 126.6, 127.2, 127.6, 127.8, 129.1, 129.6, 130.0, 134.8, 138.3, 141.7, 145.6 (aromatic carbons), 161.6, 166.2 (2 C=O); MS,  $m/z$  [%]: 485.30 [ $\text{M}^+$ +2, 17.85], 483.30 [ $\text{M}^+$ , 48.45]; Anal. Calcd. for  $\text{C}_{22}\text{H}_{18}\text{ClN}_5\text{O}_4\text{S}$  (483.93): C, 54.60; H, 3.75; N, 14.47. Found: C, 54.51; H, 3.89; N, 14.70.

**2.1.2.7. *N*-(2-Bromophenyl)-2-(2-oxo-3-(2-(4-sulfamoylphenyl)hydrazono)indolin-1-yl) acetamide (3g).** Yellow crystals, yield 73%, m.p. 279–280 °C; IR (KBr,  $\nu$   $\text{cm}^{-1}$ ): 3364, 3333, 3155 ( $\text{NH}_2$ , 2NH), 3059 (CH aromatic), 2974, 2935 (CH aliphatic), 1697 (2 C=O), 1597 (NH bending), 1570, 1539 (C=C), 1300, 1153 ( $\text{SO}_2$ );  $^1\text{H}$  NMR (DMSO- $d_6$ , 400 MHz):  $\delta$  4.71, 4.76 (2s, 2H,  $\text{NCH}_2$ ), 7.10 (d,  $J$  = 7.84 Hz, 1H, aromatic H), 7.14–7.19 (m, 2H, aromatic H), 7.27, 7.25 (2s, 2H,  $\text{NH}_2$ ,  $\text{D}_2\text{O}$  exchangeable), 7.36–7.43 (m, 2H, aromatic H), 7.57–7.69 (m, 4H, aromatic H), 7.82 (d,  $J$  = 8.48 Hz, 2H, aromatic H), 8.31 (d,  $J$  = 7.60 Hz, 1H, aromatic H), 9.93, 10.87 (2s, 1H, NH,  $\text{D}_2\text{O}$  exchangeable), 9.97, 12.66 (2s, 1H, NH,  $\text{D}_2\text{O}$  exchangeable);  $^{13}\text{C}$  NMR (DMSO- $d_6$ , 100 MHz):  $\delta$  42.7, 43.0 ( $\text{NCH}_2$ ), 109.7, 110.2, 114.5, 115.1, 116.0, 118.6, 119.4, 120.6, 122.5, 123.2, 127.7, 127.9, 128.6, 129.2, 129.7, 131.2, 133.2, 136.2, 138.0, 138.3, 141.7, 143.1, 145.6, 147.2 (aromatic carbons), 161.6, 164.5, 166.1, 166.2 (C=O); MS,  $m/z$  [%]: 530 [ $\text{M}^+$ +2, 13.24], 528 [ $\text{M}^+$ , 13.20]; Anal. Calcd. for  $\text{C}_{22}\text{H}_{18}\text{BrN}_5\text{O}_4\text{S}$  (528.38): C, 50.01; H, 3.43; N, 13.25. Found: C, 50.28; H, 3.61; N, 13.19.

### 2.1.3. General procedure for the synthesis of compounds 4a-g

A mixture of equimolar amounts of (**2a-g**) (1 mmol) and 4-((2-hydrazinyl-2-oxoethyl)amino)benzenesulfonamide (0.24 g, 1 mmol)

was dissolved in methanol (5 ml) in the presence of glacial acetic acid (0.5 ml) and stirred at room temperature for 3 h. The obtained precipitate was filtered, washed with ethanol and recrystallized from ethanol.

**2.1.3.1. 2-(2-Oxo-3-(2-(2-(4-sulfamoylphenylamino)acetyl)hydrazono)indolin-1-yl)-*N*-phenylacetamide (4a).** Yellow crystals, yield 80%, m.p. 272–273 °C; IR (KBr,  $\nu$   $\text{cm}^{-1}$ ): 3379, 3283, 3237, 3144 ( $\text{NH}_2$ , 3NH), 3071 (CH aromatic), 2978, 2939 (CH aliphatic), 1720, 1693, 1663 (3 C=O), 1601 (NH bending), 1550, 1516 (C=C), 1312, 1150 ( $\text{SO}_2$ );  $^1\text{H}$  NMR (DMSO- $d_6$ , 400 MHz):  $\delta$  4.38 (s, 2H,  $\text{NHCH}_2$ ), 4.64 (s, 2H,  $\text{NCH}_2$ ), 6.71–6.79 (m, 3H, aromatic H), 6.95 (s, 2H,  $\text{NH}_2$ ,  $\text{D}_2\text{O}$  exchangeable), 7.06–7.15 (m, 3H, aromatic H), 7.32 (t,  $J$  = 7.90 Hz, 2H, aromatic H), 7.47 (t,  $J$  = 7.63 Hz, 1H, aromatic H), 7.54–7.59 (m, 4H, aromatic H), 8.13 (s, 1H, NH,  $\text{D}_2\text{O}$  exchangeable), 10.35 (s, 1H, NH,  $\text{D}_2\text{O}$  exchangeable), 11.41 (s, 1H, NH,  $\text{D}_2\text{O}$  exchangeable);  $^{13}\text{C}$  NMR (DMSO- $d_6$ , 100 MHz):  $\delta$  43.2, 43.3 (2  $\text{CH}_2$ ), 110.2, 111.8, 115.2, 119.7, 123.8, 124.1, 126.3, 127.8, 133.1, 138.9, 139.0, 143.8, 144.9, 151.5 (aromatic carbons), 164.1, 165.2, 165.5 (3 C=O); MS,  $m/z$  [%]: 507.79 [ $\text{M}^+$ +1, 15]; Anal. Calcd. for  $\text{C}_{24}\text{H}_{22}\text{N}_6\text{O}_5\text{S}$  (506.53): C, 56.91; H, 4.38; N, 16.59. Found: C, 57.12; H, 4.60; N, 16.78.

**2.1.3.2. *N*-(4-Chlorophenyl)-2-(2-oxo-3-(2-(2-(4-sulfamoylphenylamino)acetyl)hydrazono)indolin-1-yl)acetamide (4b).** Yellow crystals, yield 78%, m.p. 270–271 °C; IR (KBr,  $\nu$   $\text{cm}^{-1}$ ): 3333, 3294, 3206, 3136 ( $\text{NH}_2$ , 3NH), 3063–3032 (CH aromatic), 2978, 2947 (CH aliphatic), 1716, 1693, 1659 (3 C=O), 1612 (NH bending), 1554, 1512 (C=C), 1319, 1149 ( $\text{SO}_2$ );  $^1\text{H}$  NMR (DMSO- $d_6$ , 400 MHz):  $\delta$  4.37 (s, 2H,  $\text{NHCH}_2$ ), 4.58, 4.64 (2s, 2H,  $\text{NCH}_2$ ), 6.61 (d,  $J$  = 8.52 Hz, 2H, aromatic H), 6.72 (d,  $J$  = 8.48 Hz, 1H, aromatic H), 6.94, 6.95 (2s, 2H,  $\text{NH}_2$ ,  $\text{D}_2\text{O}$  exchangeable), 7.11, 7.20 (m, 2H, aromatic H), 7.38 (d,  $J$  = 8.76 Hz, 2H, aromatic H), 7.45 (d,  $J$  = 7.60 Hz, 1H, aromatic H), 7.51–7.63 (m, 3H, aromatic H), 7.67 (t,  $J$  = 7.74 Hz, 1H, aromatic H), 8.12 (s, 1H, NH,  $\text{D}_2\text{O}$  exchangeable), 10.36, 10.49 (2s, 1H, NH,  $\text{D}_2\text{O}$  exchangeable), 11.37 (s, 1H, NH,  $\text{D}_2\text{O}$  exchangeable);  $^{13}\text{C}$  NMR (DMSO- $d_6$ , 100 MHz):  $\delta$  43.6, 45.0 (2  $\text{CH}_2$ ), 111.4, 115.2, 117.9, 121.3, 121.6, 124.1, 125.0, 127.7, 129.2, 131.2, 137.7, 138.9, 144.7, 151.1, 158.9 (aromatic carbons), 165.7, 169.3, 183.4 (3 C=O); MS,  $m/z$  [%]: 542.94 [ $\text{M}^+$ +2, 32.72], 540.88 [ $\text{M}^+$ , 40]; Anal. Calcd. for  $\text{C}_{24}\text{H}_{21}\text{ClN}_6\text{O}_5\text{S}$  (540.98): C, 53.28; H, 3.91; N, 15.53. Found: C, 53.61; H, 4.08; N, 15.79.

**2.1.3.3. *N*-(3-Bromophenyl)-2-(2-oxo-3-(2-(2-(4-sulfamoylphenylamino)acetyl)hydrazono)indolin-1-yl)acetamide (4c).** Orange yellow crystals, yield 78%, m.p. 260–262 °C; IR (KBr,  $\nu$   $\text{cm}^{-1}$ ): 3329, 3294, 3236, 3198 ( $\text{NH}_2$ , 3NH), 3067, 3032 (CH aromatic), 2947, 2897 (CH aliphatic), 1725, 1697, 1650 (3 C=O), 1600 (NH bending), 1550, 1512 (C=C), 1315, 1149 ( $\text{SO}_2$ );  $^1\text{H}$  NMR (DMSO- $d_6$ , 400 MHz):  $\delta$  4.36 (s, 2H,  $\text{NHCH}_2$ ), 4.58, 4.64 (2s, 2H,  $\text{NCH}_2$ ), 6.61, 6.71 (2d,  $J$  = 8.44 Hz, 2H, aromatic H), 6.91, 7.11 (2d,  $J$  = 8.10 Hz, 1H, aromatic H), 6.94, 6.95 (2s, 2H,  $\text{NH}_2$ ,  $\text{D}_2\text{O}$  exchangeable), 7.03, 7.17 (2t,  $J$  = 7.68 Hz, 1H, aromatic H), 7.45, 7.67 (2t,  $J$  = 7.70 Hz, 1H, aromatic H), 7.47–7.56 (m, 6H, aromatic H), 7.62 (d,  $J$  = 7.36 Hz, 1H, aromatic H), 8.12 (s, 1H, NH,  $\text{D}_2\text{O}$  exchangeable), 10.37, 10.49 (2s, 1H, NH,  $\text{D}_2\text{O}$  exchangeable), 11.37 (s, 1H, NH,  $\text{D}_2\text{O}$  exchangeable);  $^{13}\text{C}$  NMR (DMSO- $d_6$ , 100 MHz):  $\delta$  43.4, 43.7, 45.0 (2  $\text{CH}_2$ ), 111.5, 111.7, 115.7, 115.9, 117.9, 121.3, 121.6, 121.9, 122.2, 122.8, 124.0, 125.0, 126.3, 126.5, 127.7, 127.8, 131.2, 132.1, 138.1, 138.3, 138.8, 143.7, 144.7, 151.2, 151.4, 151.5, 158.9 (aromatic carbons), 165.5, 169.2, 183.3 (C=O); MS,  $m/z$  [%]: 583.20 [ $\text{M}^+$ -2, 1.84]; Anal. Calcd. For

$C_{24}H_{21}BrN_6O_5S$  (585.43): C, 49.24; H, 3.62; N, 14.36. Found: C, 49.52; H, 3.83; N, 14.59.

**2.1.3.4. 2-(2-Oxo-3-(2-(2-(4-sulfamoylphenylamino)acetyl)hydrazono)indolin-1-yl)-N-m-tolylacetamide (4d).** Yellow crystals, yield 75%, m.p. 273–274 °C; IR (KBr,  $\nu$   $cm^{-1}$ ): 3344, 3294 (NH<sub>2</sub>, 3NH), 3032 (CH aromatic), 2974, 2897 (CH aliphatic), 1717, 1697, 1659 (3 C=O), 1597 (NH bending), 1512 (C=C), 1315, 1145 (SO<sub>2</sub>); <sup>1</sup>H NMR (DMSO-d<sub>6</sub>, 400 MHz):  $\delta$  2.26 (s, 3H, CH<sub>3</sub>), 4.37 (s, 2H, NHCH<sub>2</sub>), 4.62 (s, 2H, NCH<sub>2</sub>), 6.61, 6.71 (2d,  $J$  = 8.60 Hz, 2H, aromatic H), 6.94, 6.95 (2s, 2H, NH<sub>2</sub>, D<sub>2</sub>O exchangeable), 7.10–7.14 (m, 4H, aromatic H), 7.44 (d,  $J$  = 8.04 Hz, 2H, aromatic H), 7.49 (d,  $J$  = 8.76 Hz, 2H, aromatic H), 7.55 (d,  $J$  = 8.72 Hz, 2H, aromatic H), 8.12 (s, 1H, NH, D<sub>2</sub>O exchangeable), 9.16 (s, 1H, NH, D<sub>2</sub>O exchangeable), 10.25 (s, 1H, NH, D<sub>2</sub>O exchangeable); <sup>13</sup>C NMR (DMSO-d<sub>6</sub>, 100 MHz):  $\delta$  20.9 (CH<sub>3</sub>), 43.3, 45.0 (2CH<sub>2</sub>), 110.2, 111.6, 111.7, 115.2, 119.8, 122.8, 126.3, 127.8, 129.7, 131.2, 133.0, 136.5, 143.8, 144.9, 151.5 (aromatic carbons), 165.3, 169.2, 173.1 (3 C=O); MS,  $m/z$  [%]: 522.38 [ $M^+$ +2, 18], 520.41 [ $M^+$ , 19]; Anal. Calcd. For C<sub>25</sub>H<sub>24</sub>N<sub>6</sub>O<sub>5</sub>S (520.56): C, 57.68; H, 4.65; N, 16.14. Found: C, 57.96; H, 4.82; N, 16.36.

**2.1.3.5. N-(3-Methoxyphenyl)-2-(2-oxo-3-(2-(2-(4-sulfamoylphenylamino)acetyl)hydrazono)indolin-1-yl)acetamide (4e).** Yellow crystals, yield 70%, m.p. 278–279 °C; IR (KBr,  $\nu$   $cm^{-1}$ ): 3379, 3329, 3290, 3233 (NH<sub>2</sub>, 3NH), 3074 (CH aromatic), 2974, 2901 (CH aliphatic), 1720, 1693, 1659 (3 C=O), 1601 (NH bending), 1512 (C=C), 1311, 1149 (SO<sub>2</sub>); <sup>1</sup>H NMR (DMSO-d<sub>6</sub>, 400 MHz):  $\delta$  3.72 (s, 3H, OCH<sub>3</sub>), 4.37 (s, 2H, NHCH<sub>2</sub>), 4.60 (s, 2H, NCH<sub>2</sub>), 6.70–6.73 (m, 2H, aromatic H), 6.89 (d,  $J$  = 9.00 Hz, 2H, aromatic H), 6.95, 6.97 (2s, 2H, NH<sub>2</sub>, D<sub>2</sub>O exchangeable), 7.10–7.21 (m, 3H, aromatic H), 7.45–7.50 (m, 3H, aromatic H), 7.55 (d,  $J$  = 7.64 Hz, 2H, aromatic H), 8.12 (s, 1H, NH, D<sub>2</sub>O exchangeable), 10.19 (s, 1H, NH, D<sub>2</sub>O exchangeable), 11.40 (s, 1H, NH, D<sub>2</sub>O exchangeable); <sup>13</sup>C NMR (DMSO-d<sub>6</sub>, 100 MHz):  $\delta$  43.1, 43.3 (2CH<sub>2</sub>), 55.6 (OCH<sub>3</sub>), 110.2, 111.8, 114.4, 115.2, 121.3, 122.8, 123.7, 126.3, 127.8, 132.1, 133.0, 143.8, 144.9, 151.4, 155.9 (aromatic carbons), 164.0, 164.5, 165.0 (3 C=O); MS,  $m/z$  [%]: 536.20 [ $M^+$ , 40]; Anal. Calcd. For C<sub>25</sub>H<sub>24</sub>N<sub>6</sub>O<sub>6</sub>S (536.56): C, 55.96; H, 4.51; N, 15.66. Found: C, 56.13; H, 4.67; N, 15.89.

**2.1.3.6. N-(2-Chlorophenyl)-2-(2-oxo-3-(2-(2-(4-sulfamoylphenylamino)acetyl)hydrazono)indolin-1-yl)acetamide (4f).** Yellow crystals, yield 65%, m.p. 206–208 °C; IR (KBr,  $\nu$   $cm^{-1}$ ): 3379, 3283, 3256 (NH<sub>2</sub>, 3NH), 3066 (CH aromatic), 2927, 2835 (CH aliphatic), 1740, 1720, 1674 (3 C=O), 1597 (NH bending), 1539, 1520 (C=C), 1312, 1150 (SO<sub>2</sub>); <sup>1</sup>H NMR (DMSO-d<sub>6</sub>, 400 MHz):  $\delta$  3.69, 3.70 (2s, 2H, NHCH<sub>2</sub>), 4.26, 4.32 (2s, 1H, NH, D<sub>2</sub>O exchangeable), 4.46, 4.71 (2s, 2H, NCH<sub>2</sub>), 6.61 (d,  $J$  = 8.68 Hz, 2H, aromatic H), 6.70 (d,  $J$  = 8.72 Hz, 2H, aromatic H), 6.93 (s, 2H, NH<sub>2</sub>, D<sub>2</sub>O exchangeable), 7.08 (d,  $J$  = 7.68 Hz, 1H, aromatic H), 7.11 (d,  $J$  = 7.56 Hz, 1H, aromatic H), 7.23 (t,  $J$  = 6.96 Hz, 1H, aromatic H), 7.33 (t,  $J$  = 7.36 Hz, 1H, aromatic H), 7.42–7.46 (m, 1H, aromatic H), 7.51 (d,  $J$  = 8.72 Hz, 2H, aromatic H), 7.70 (d,  $J$  = 7.12 Hz, 1H, aromatic H), 9.15 (s, 1H, NH, D<sub>2</sub>O exchangeable), 9.96 (s, 1H, NH, D<sub>2</sub>O exchangeable); <sup>13</sup>C NMR (DMSO-d<sub>6</sub>, 100 MHz):  $\delta$  45.03, 46.07 (2CH<sub>2</sub>), 111.64, 111.83, 122.84, 127.6, 127.8, 128.0, 128.3, 130.0, 131.2, 131.7, 132.1, 133.5, 134.8, 135.3, 138.1, 151.5 (aromatic carbons), 159.2, 169.2 (C=O); MS,  $m/z$  [%]: 541.10 [ $M^+$ +1, 1.63], 539.10 [ $M^+$ -1, 2.34]; Anal. Calcd. For C<sub>24</sub>H<sub>21</sub>ClN<sub>6</sub>O<sub>5</sub>S (540.98): C, 53.28; H, 3.91; N, 15.53. Found: C, 53.44; H, 4.07; N, 15.76.

**2.1.3.7. N-(2-Bromophenyl)-2-(2-oxo-3-(2-(2-(4-sulfamoylphenylamino)acetyl)hydrazono)indolin-1-yl)acetamide (4g).** Buff crystals, yield 70%, m.p. 216–217 °C; IR (KBr,  $\nu$   $cm^{-1}$ ): 3379, 3345, 3283 (NH<sub>2</sub>, 3NH), 3062, 3032 (CH aromatic), 2920, 2850 (CH aliphatic), 1728, 1720, 1662 (3 C=O), 1601 (NH bending), 1520 (C=C), 1315, 1149 (SO<sub>2</sub>); <sup>1</sup>H NMR (DMSO-d<sub>6</sub>, 400 MHz):  $\delta$  4.15, 4.16 (2s, 2H, NHCH<sub>2</sub>), 4.62, 4.66 (2s, 2H, NCH<sub>2</sub>), 6.33, 8.99 (2s, 1H, NH, D<sub>2</sub>O exchangeable), 6.61 (d,  $J$  = 8.68 Hz, 2H, aromatic H), 6.69 (d,  $J$  = 8.72 Hz, 2H, aromatic H), 6.89, 6.93 (2s, 2H, NH<sub>2</sub>, D<sub>2</sub>O exchangeable), 6.98, 8.36 (2d,  $J$  = 7.32 Hz, 1H, aromatic H), 7.12–7.20 (m, 2H, aromatic H), 7.38 (t,  $J$  = 7.62 Hz, 1H, aromatic H), 7.51 (d,  $J$  = 8.48 Hz, 2H, aromatic H), 7.61–7.70 (m, 2H, aromatic H), 9.21, 9.59 (2s, 1H, NH, D<sub>2</sub>O exchangeable), 9.81, 10.02 (2s, 1H, NH, D<sub>2</sub>O exchangeable); <sup>13</sup>C NMR (DMSO-d<sub>6</sub>, 100 MHz):  $\delta$  42.85, 45.05 (2CH<sub>2</sub>), 111.5, 115.2, 118.8, 122.0, 125.1, 127.3, 127.6, 127.7, 128.6, 130.2, 131.2, 133.2, 136.4, 151.8 (aromatic carbons), 167.0, 173.9, 181.3 (3 C=O); MS,  $m/z$  [%]: 585.20 [ $M^+$ , 0.90], 583.20 [ $M^+$ -2, 1.38]; Anal. Calcd. For C<sub>24</sub>H<sub>21</sub>BrN<sub>6</sub>O<sub>5</sub>S (585.43): C, 49.24; H, 3.62; N, 14.36. Found: C, 49.45; H, 3.74; N, 14.63.

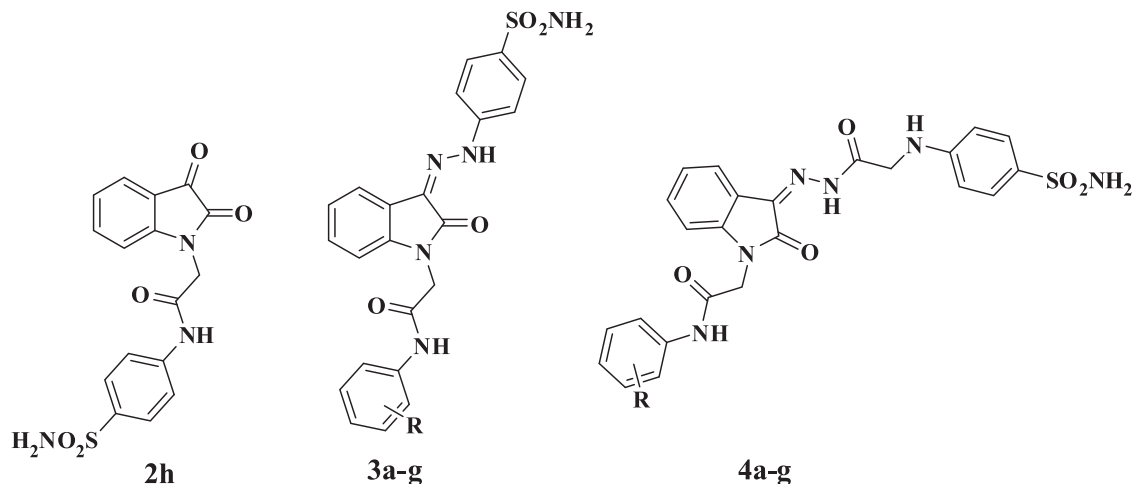
## 2.2. Carbonic anhydrase inhibitory activity

An Applied Photophysics stopped-flow instrument has been used for assaying the CA catalysed CO<sub>2</sub> hydration activity<sup>38</sup>. Phenol red (at a concentration of 0.2 mM) has been used as indicator, working at the absorbance maximum of 557 nm, with 20 mM Hepes (pH 7.5) as buffer, and 20 mM Na<sub>2</sub>SO<sub>4</sub> (for maintaining constant the ionic strength), following the initial rates of the CA-catalysed CO<sub>2</sub> hydration reaction for a period of 10–100 s. The CO<sub>2</sub> concentration ranged from 1.7 to 17 mM for the determination of the kinetic parameters and inhibition constants. For each inhibitor at least six traces of the initial 5–10% of the reaction have been used for determining the initial velocity. The uncatalysed rates were determined in the same manner and subtracted from the total observed rates. Stock solutions of inhibitor (0.1 mM) were prepared in distilled-deionized water and dilutions up to 0.01 nM were done thereafter with the assay buffer. Inhibitor and enzyme solutions were preincubated together at room temperature (15 min) prior to assay, in order to allow for the formation of the E-I complex. Data from Table 1 were obtained after 15 min incubation of enzyme and inhibitor, as for the sulphonamides reported earlier<sup>39</sup>. The inhibition constants were obtained by non-linear least-squares methods using PRISM 3 and the Cheng-Prusoff equation, as reported earlier<sup>40,41</sup> and represent the mean from at least three different determinations. All CA isoforms were recombinant ones obtained in-house as reported earlier<sup>42</sup>.

## 2.3. Anti-proliferative activity

Cancer cell lines were obtained from Nawah Scientific Inc. (Mokatam, Cairo, Egypt). Cells were maintained in DMEM media supplemented with 100 mg/mL of streptomycin, 100 units/mL of penicillin and 10% of heat-inactivated foetal bovine serum in humidified, 5%(v/v) CO<sub>2</sub> atmosphere at 37 °C.

Cell viability assay was assessed by SRB assay. Aliquots of 100  $\mu$ L cells suspension ( $5 \times 10^3$  cells) were in 96 well plates and incubated in complete media for 24 h. Cells were treated with another aliquot of 100  $\mu$ L media containing drugs at various concentrations. After 72 h of drug exposure, cells were fixed by replacing media with 150  $\mu$ L of 10% TCA and incubated at 4 °C for 1 h. The TCA solution was removed, and the cells were washed 5 times with distilled water. Aliquots of 70  $\mu$ L SRB solution (0.4% w/v) were added and incubated in a dark place at room temperature

**Table 1.** Inhibition data of human CA isoforms *hCA* I, II, IX and XII with 2,3-dioxindole sulfamoylphenyl acetamide **2h**, 2-oxindole based benzenesulfonamides **3a-g**, **4a-g** and the standard inhibitor Acetazolamide (AAZ) using a stopped flow CO<sub>2</sub> hydrase assay.

Compound ID	R	$K_i^a$ (nM)				Selectivity ratio			
		<i>hCA</i> I	<i>hCA</i> II	<i>hCA</i> IX	<i>hCA</i> XII	I/IX	II/IX	I/XII	II/XII
<b>2h</b>	SO <sub>2</sub> NH <sub>2</sub>	45.1	5.87	67.0	7.91	0.673	0.087	5.701	0.742
<b>3a</b>	H	3971	260	216	3649	18.384	1.203	1.088	0.071
<b>3b</b>	4-Cl	892	452	123	474	7.252	3.674	1.881	0.953
<b>3c</b>	4-Br	762	56.4	56.9	612	13.392	0.991	1.245	0.092
<b>3d</b>	4-CH <sub>3</sub>	656	79.9	85.5	710	7.672	0.934	0.923	0.112
<b>3e</b>	4-OCH <sub>3</sub>	776	180	598	599	1.297	0.301	1.295	0.300
<b>3f</b>	2-Cl	2695	804	673	3295	4.004	1.194	0.817	0.244
<b>3g</b>	2-Br	708	420	401	766	1.765	1.047	0.924	0.548
<b>4a</b>	H	4639	804	808	6792	5.741	0.995	0.683	0.118
<b>4b</b>	4-Cl	8429	4586	3922	5045	2.149	1.169	1.670	0.909
<b>4c</b>	4-Br	2352	732	654	2285	3.596	1.119	1.029	0.320
<b>4d</b>	4-CH <sub>3</sub>	8509	458	574	6025	14.824	0.797	1.412	0.076
<b>4e</b>	4-OCH <sub>3</sub>	9318	6722	3151	1522	2.957	2.133	6.122	4.416
<b>4f</b>	2-Cl	4391	2969	5358	754	0.819	0.554	5.823	3.937
<b>4g</b>	2-Br	6088	2001	7336	843	0.829	0.272	7.221	2.373
<b>AAZ</b>	—	250.0	12.0	25.0	5.7	10	0.48	43.859	2.105

<sup>a</sup>Mean from 3 different assays, by a stopped flow technique (errors were in the range of  $\pm$  5–10% of the reported values).

for 10 min. Plates were washed 3 times with 1% acetic acid and allowed to air-dry overnight. Then, 150  $\mu$ L of TRIS (10 mM) was added to dissolve protein-bound SRB stain; the absorbance was measured at 540 nm using a BMGLABTECH<sup>®</sup> -FLUO star Omega microplate reader (Ortenberg, Germany)<sup>43,44</sup>. All experiments were performed in triplicate wells for each condition. IC<sub>50</sub> values were calculated from concentration-response curves by Sigma Plot software, version 12.0 (System Software, San Jose, CA, USA), using an E-max model equation. Also selectivity index was determined.

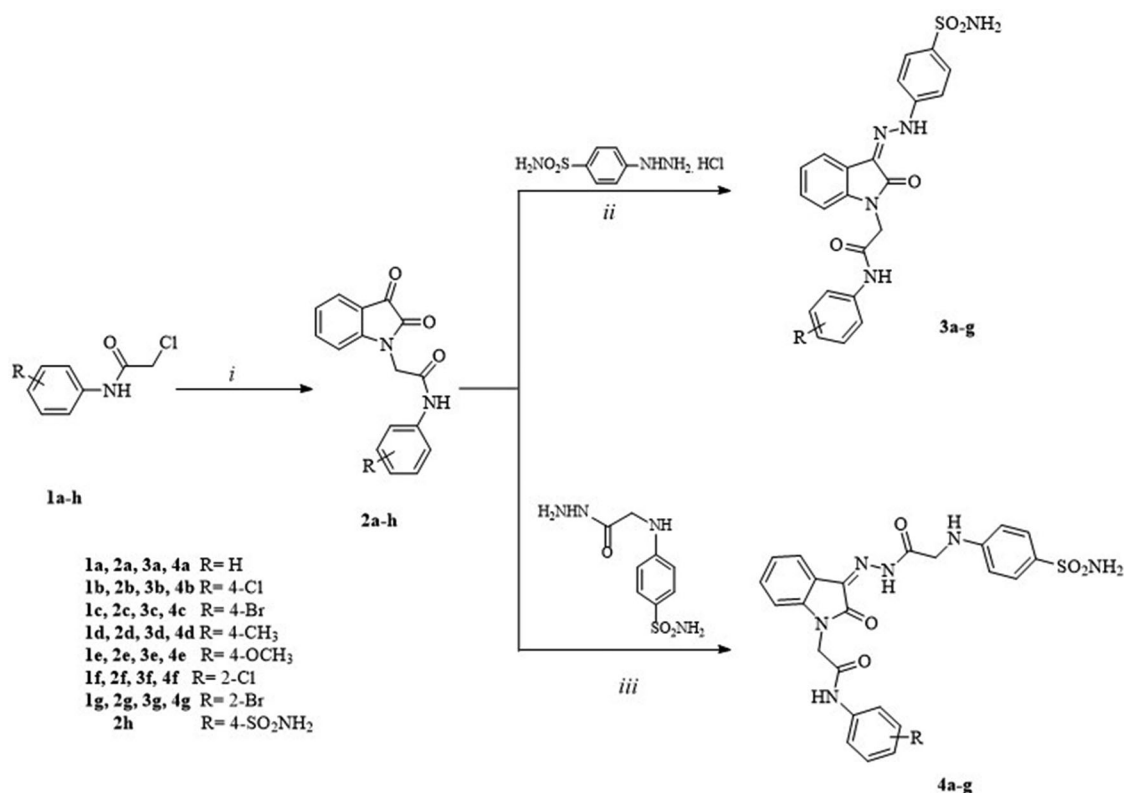
#### 2.4. Molecular docking

Molecular Operating Environment MOE<sup>®</sup> 2014.0901 was used as the computational software throughout the docking study. The best quality chains of the four PDB files (3W6H, 3HS4, 3IAI and 1JD0 for *hCA* I, II, IX and XII, respectively) were selected where the unnecessary ions, ligands and water molecules were removed in a radius of 4.0 Å. The 3D protein structures were protonated using their corresponding pH and temperature conditions. The selected compounds **2h** and **3c** were constructed then deprotonated *in-silico* using amber:10EHT forcefield followed by energy minimisation at a gradient of 0.01 RMSD. On the fly-docking protocol was implemented at the same forcefield using triangle matcher, London dG and GBVI/WSA dG as placement and rescoring function 1 and 2, respectively.

For accurate molecular docking protocol, validation was done by self-docking the co-crystallised ligands to get the lowest root mean square deviation (RMSD) and the highest energy score (S).

#### 2.5. 2D-QSAR study

The compounds were constructed, and energy minimised using MOE<sup>®</sup> 2014.0901 MMFF94x forcefield at the default parameters with RMS gradient 0.1 Kcal/mol/Å<sup>2</sup> then divided into training and testing sets for model generation and validation, respectively. For *hCA* IX, 34 compounds were used as the training set and 5 as test set of compounds while for *hCA* XII, 34 and 6 compounds were used as the training and test set, respectively. A variety of 413 1D and 2D descriptors were calculated using Chemopy<sup>®</sup> descriptors from ChemDes<sup>®</sup> open-source webserver. Thereafter, descriptors with constant values across the training set or equal to zero were excluded. RapidMiner<sup>®</sup> Studio 9.10 program was used for descriptors filtration through the forward selection optimisation algorithm against the dependent variable log  $K_i$  then the best descriptors were transferred back to MOE<sup>®</sup> for a linear model generation using the partial least square (PLS) method.



**Scheme 1.** Synthetic pathway for the target compounds 1–4. **Reagents and reaction conditions.** (i) Glacial acetic acid, sodium acetate, 0 °C. (ii) MeOH, r.t. (iii) MeOH, glacial acetic acid, r.t.

### 3. Results and discussion

#### 3.1. Chemistry

Scheme 1 illustrates the synthesis of the target 2-oxindole benzenesulfonamide analogs **3a-g** and **4a-g**. Known 2-chloro-*N*-[(un)sub]phenylacetamides (**1a-h**) were prepared according to the reported method by alkylation of the appropriate substituted aniline derivatives with chloroacetylchloride<sup>31,32</sup>. The reported key intermediates (**2a-f**)<sup>33–35</sup> and the new ones (**2g, h**) were prepared according to the conventional method by the reaction of the commercially available isatin (indole-2,3-dione) with the corresponding 2-chloro-*N*-phenacetamide (**1a-h**) in dry *N, N*-dimethyl formamide (DMF) in the presence of potassium carbonate. Then, **2a-g** were condensed with the prepared 4-hydrazinylbenzenesulfonamide hydrochloride<sup>36</sup> at room temperature to give new 4-[2-(2-oxindolin-3-ylidene)hydrazinyl]benzenesulfonamide (**3a-g**). Similarly, the condensation of **2a-g** with the prepared 4-(2-hydrazinyl-2-oxoethylamino)benzenesulfonamide<sup>37</sup> in methanol at room temperature afforded 4-(2-oxindolin-3-ylidene)hydrazinyl-2-oxoethylamino benzenesulfonamide derivatives (**4a-g**). All new derivatives were confirmed by spectral and elemental analyses as detailed in the experimental part.

It is noteworthy that all target compounds **3a-g** and **4a-g** contain an exocyclic C=N imine bond which results in their presence as *E/Z* geometrical isomers. However, it was reported that *E/Z* ratio is dependent on each isomer stability and NMR solvent<sup>28,45,46</sup>. This fact was observed in many compounds like **3a,b,f,g** and **4b,c,f,g** which were found in a mixture of *E* and *Z* isomers as observed from their <sup>1</sup>H NMR spectra that revealed additional signals due to both isomers. For instance, <sup>1</sup>H NMR spectrum of compound **3a** had two singlets attributed to the methylene protons at 4.65 ppm (*E*-isomer) and 4.70 ppm (*Z*-isomer) with integration

ratio 3.23:3.42, respectively, whereas compounds **3c,d,e** showed both isomeric forms with integration ratio (6:1) for *Z*-isomer. On the other hand, compounds **4a,d,e** were isolated mainly as *Z* isomers. (see the experimental section).

#### 3.2. Carbonic anhydrase inhibitory activity

The new candidates 2,3-dioxindole sulfamoylphenyl acetamide **2h**, 2-oxindole derivatives (hydrazinyl benzenesulfonamide (**3a-g**) and hydrazinyl 2-oxoethylamino benzenesulfonamide congeners (**4a-g**) were evaluated for their ability to inhibit four physiologically relevant *hCA* isoforms (cytosolic isoforms; *hCA* I, *hCA* II and the transmembrane, tumour-associated isoforms *hCA* IX, *hCA* XII) through a stopped flow CO<sub>2</sub> hydrase assay<sup>38–42</sup>. Their potency as *K<sub>i</sub>* (nM) were compared to the standard CA inhibitor acetazolamide (AAZ) and these results were summarised in (Table 1). A brief study of SAR revealed the followings:

- Regarding the ability of the tested compounds to inhibit *hCA* I, all tested compounds except **2h** revealed relatively lower activity than other isoforms. It was noticed that 2,3-dioxindole **2h** showed an extremely high potency (*K<sub>i</sub>* = 45.1 nM) compared to AAZ (*K<sub>i</sub>* = 250 nM) and to other tested compounds that showed inhibitory activity ranged from 656 to 9318 nM. Derivatives linked to hydrazinyl benzenesulfonamide (**3a-g**) were more active (*K<sub>i</sub>* = 656–3971 nM) than their analogs linked to hydrazinyl 2-oxoethylamino benzenesulfonamide congeners (**4a-g**) (*K<sub>i</sub>* = 2353–9318 nM). Also, in hydrazinyl benzenesulfonamides (**3a-g**) substituted phenylacetamide moiety revealed activity better than unsubstituted congener, the order of activity was (4-CH<sub>3</sub> > 4-Br > 4-OCH<sub>3</sub> > 4-Cl > 2-Br > 2-Cl > H), thus, the inductive effect of



substituents at the phenyl ring has no absolute impact on the activity. On the other hand, in hydrazinyl 2-oxoethylamino benzenesulfonamide congeners (**4a-g**) the order of activity was 4-Br > 2-Cl > H > 2-Br > 4-Cl > 4-CH<sub>3</sub> > 4-OCH<sub>3</sub>, that the presence of electron withdrawing groups is more favourable for activity than electron donating moieties.

- ii. Activity towards *hCA* II isoform was better with  $K_i$  ranged from 5.87 to 4586 nM; like *hCA* I, compound **2h** was also the most potent one with  $K_i = 5.87$  nM. Derivatives linked to hydrazinyl benzenesulfonamides (**3a-g**) were more active ( $K_i = 56.4$ –804 nM) than their analogs linked to hydrazinyl 2-oxoethylamino benzenesulfonamide congeners (**4a-g**) ( $K_i = 458$ –4586 nM). In both series (**3a-g**) and (**4a-g**) it was obvious that substitution of phenylacetamide with 4-Br or 4-CH<sub>3</sub> was preferable for activity.
- iii. All the tested compounds except compounds **2h**, and **4e-g** represented a reasonable selectivity towards tumour isoform *hCA* IX compared to *hCA* I isoform. The hydrazinyl benzenesulfonamide (**3a-g**) were more active ( $K_i = 56.9$ –673 nM) than their analogs linked to hydrazinyl 2-oxoethylamino benzenesulfonamide congeners (**4a-g**) ( $K_i = 574$ –7336 nM). The 4-bromophenylacetamide derivative (**3c**) was the most active one. Similar to *hCA* II activity, in both series (**3a-g**) and (**4a-g**) it was obvious that substitution of phenylacetamide with 4-Br or 4-CH<sub>3</sub> was preferable for activity.
- iv. Regarding the *hCA* XII inhibition, all the tested compounds except compounds **2h**, revealed very weak selectivity towards *hCA* XII. Compound **2h** was relatively the most potent one with  $K_i = 7.91$  nM. Hydrazinyl benzenesulfonamide (**3a-g**) were more active than their analogs linked to hydrazinyl 2-oxoethylamino benzenesulfonamide congeners (**4a-g**). In hydrazinyl benzenesulfonamide (**3a-g**) it was obvious that substitution of phenylacetamide with 4-Br or 4-Cl was preferable for activity, while in hydrazinyl 2-oxoethylamino benzenesulfonamide congeners (**4a-g**) substitution at ortho position of phenylacetamide with Br or Cl was more favoured.
- v. Finally, from our previous studies to develop isatin-based CA derivatives<sup>29,30</sup> we can find in the current study that the presence of substituted phenylacetamide increase the potency specially for *hCA* I and shifted the selectivity mainly towards *hCA* IX comparing to substituted benzoyl moiety in the previous study<sup>30</sup> that reflects the ability of these compounds to have promising anticancer activity. Also, in our current study increasing the length of the *N*-substitution from *N*-benzoyl to *N*-phenylacetamido group leading to decrease in potency mainly against all isoforms and slightly shifted the selectivity in case of 2-substituted phenylacetamide analogs.

### 3.3. Anti-proliferative activity

As CA IX is overexpressed in MCF-7 breast cancer cell line<sup>47</sup> and in A549 lung cancer cells<sup>48</sup>, therefore, compounds **2h**, **3c** and **3d** eliciting the best CA IX inhibition were selected for further evaluation for their anti-proliferative activity against these cancer cell lines. Moreover, they were tested for their cytotoxicity against normal human skin fibroblast cell line HSF to confirm their safety, the results are illustrated in Table 2 and Figures S1–S6. Compound **3d** showed good cytotoxic activity against MCF-7 and A549 cell lines with  $IC_{50} = 0.869$  and  $5.12 \mu\text{M}$ , respectively. On the other hand, **3c** exerted only cytotoxic activity against A549 cell line with  $IC_{50} = 5.90 \mu\text{M}$ . Furthermore, **3c** showed promising safety margin towards normal cells through its selectivity towards A549 cells in

**Table 2.** Cytotoxic activity and selectivity index of compounds **2h**, **3c**, and **3d** on cancer and normal cell lines

Cell line	Compd.							
	$IC_{50}$ ( $\mu\text{M}$ )				Selectivity index			
	Doxorubicin	2h	3c	3d	Doxorubicin	2h	3c	3d
MCF-7	0.63	>100	>100	0.869	0.349	1	1	1.68
A549	0.19	>100	5.90	5.12	1.157	1	16.94	0.28
HSF	0.22	>100	>100	1.46	—	—	—	—

contrast to doxorubicin and **3d** which were unselectively cytotoxic to both normal and cancer cell lines. Unfortunately, compound **2h** found to have no cytotoxic activity against both cell lines, thus, its anti-proliferative activity is not correlated to its CA IX inhibition, however, it can be considered as an adjuvant with an anti-cancer agent to enhance its cytotoxic effect due to its CA IX inhibition activity similar to acetazolamide.

### 3.4. Molecular docking study

Molecular docking was done for **2h** and **3c** to relate their *in vitro* biological results with their possible conformations for binding to the four CA isoforms. Hence, the crystal structure of each isoform co-crystallised with **AAZ** was downloaded from the Protein Data Bank (PDB) using PDB ID: 3W6H, 3HS4, 3IAI and 1JD0 for isoforms *hCA* I, II, IX and XII, respectively<sup>49</sup>. Molecular docking method was validated using the co-crystallised **AAZ** by self-docking till getting the same interaction pattern with each isoform binding site residues as presented in Supplementary Figure S10a–d. Considering the importance of sulphonamide moiety deprotonation to coordinate with the positively charged zinc ion<sup>50</sup>, the tested compounds sulphonamide group were *in-silico* deprotonated and energy minimised before docking.

The molecular docking of the most active derivative **2h** augmented the achieved *in vitro*  $K_i$  values that surpassed **AAZ** using both *hCA* isoforms I and II. Considering *hCA* I (PDB ID 3W6H), it revealed the formation of the two characteristic co-ordinations with zinc ion using the deprotonated nitrogen of the sulphonamide moiety (Figure 3(a)) which translated into  $K_i$  value of 45.1 and 250.0 nM for **2h** and **AAZ**, respectively. The achieved co-ordinations were distanced by 2.01 (zinc–nitrogen) and 2.65 Å (zinc–oxygen) from zinc which are consistent with many crystallographic findings (Figure 3(b)). Moreover, the sulphonamide negatively charged deprotonated nitrogen was able to interact with the basic His200, a unique *hCA* I isoform zinc ligand<sup>51</sup>. This interaction could support the conformation of the sulphonamide moiety to approach zinc and stabilised the outcome interaction. Furthermore, two arene–H bonds were formed with Leu198, and Pro202 by the two phenyl groups beside the sulphonamide oxygen adeptness to accept the H-bond from Thr199. Another explanation of the resulted lower  $K_i$  value of **2h** than **AAZ** was that the capability of **2h** to block most of the *hCA* I active site entrance by its isatin moiety (Figure 3(c)).

Similarly, **2h** resulted in better  $K_i$  inhibitory value of *hCA* II isoform than **AAZ** exhibiting 5.87 and 12.0 nM, respectively. The binding mode of **2h** inside the active site of PDB ID 3HS4 managed to explain the achieved *in vitro* results. Its sulphonamide moiety interacted with zinc, Thr199, Thr200 and Leu198 forming four H-bonds ranging 2.26–3.2 Å and zinc co-ordination at 1.98 Å. In addition, two arene–H interactions were formed with Val121 and Phe131 using phenyl moiety of sulphonamide terminus and acetamide linkage, respectively (Figure 4(a,b)). Similar to *hCA* I, **2h** oriented in a

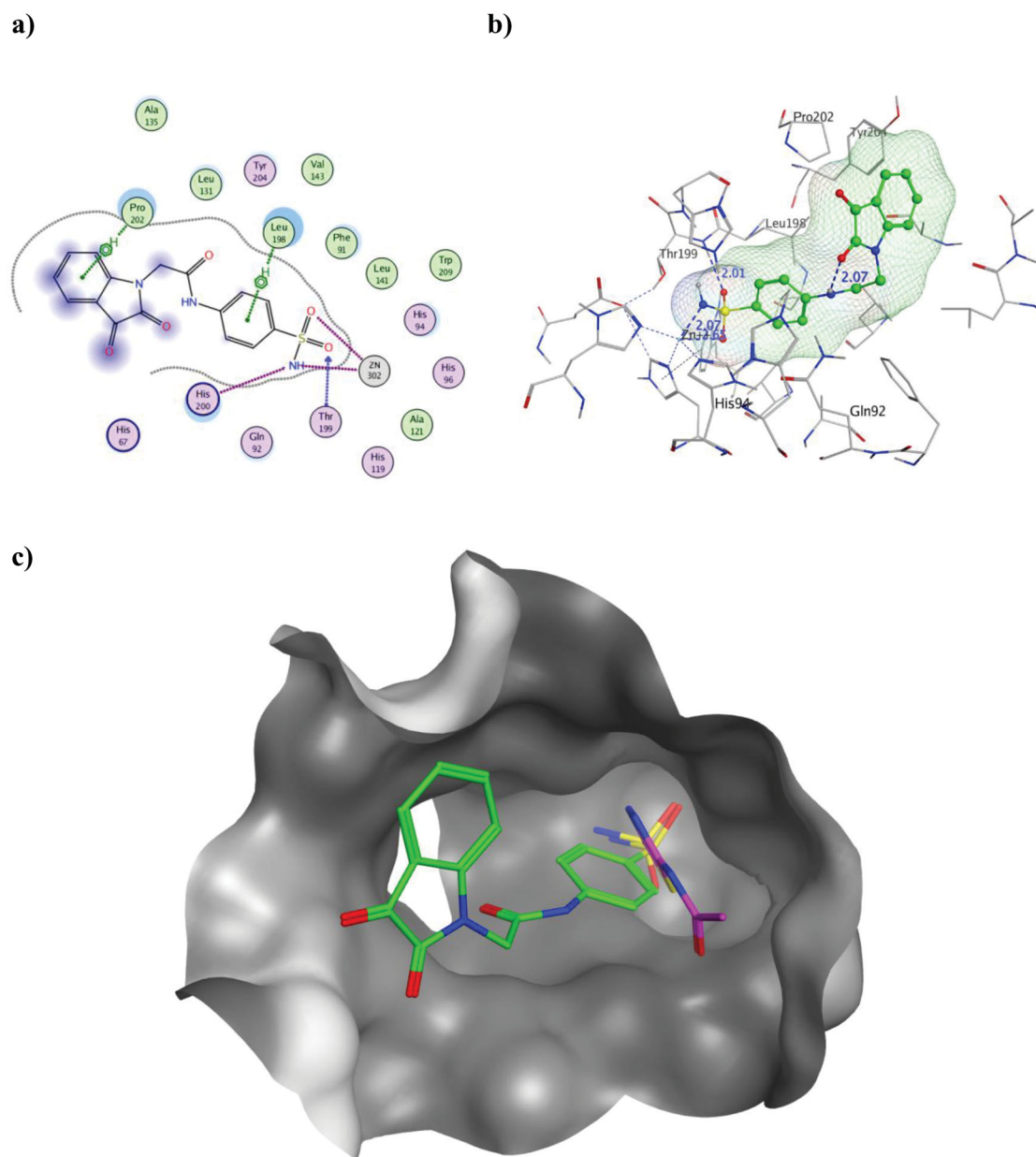


**Figure 3.** Molecular docking data of **2h** on *hCA I* isoform using PDB ID 3W6H as 2D (a) and 3D (b) presentations showing **2h** as green ball and stick model with the formed H-bonds and arene-H were shown in blue and black dotted lines, respectively with their distance in Å highlighting the interaction site. c) The overlaid 3D presentation of **2h** (green) and **AAZ** (magenta) inside the CA I active site.

conformation that blocked the entrance of *hCA II* active site by its isatin moiety (Figure 4(c)). The binding energy of **2h** was better than **AAZ** calculated as  $-10.11$  and  $-7.69$  Kcal/mol, respectively which complemented the binding conformations and achieved  $K_i$  values.

Regarding the tumour-associated *hCA IX* isoform, **2h** molecular docking data using PDB ID 3IAI showed its interaction with zinc in resemblance to other isoforms with the sulphonamide oxygen and deprotonated nitrogen suggesting good inhibitory potential (Figure 5(a)). Moreover, the oxygen atoms of sulphonamide group and acetamide linkage acted as acceptors to three H-bonds with Thr199, Thr200 and Gln92, respectively. Despite its *in silico* interaction pattern, its binding energy score was not as favourable as **AAZ** giving  $-8.75$  and  $-10.81$  Kcal/mol, respectively which explained the superiority of the achieved **AAZ**  $K_i$  value. Nonetheless, **2h** showed better  $K_i$  value on the other tested tumour-associated *hCA XII* isoform

comparing to **AAZ** showing 7.91 and 5.7 nM, respectively. Its binding mode using *hCA XII* PDB 1JD0 supported the achieved  $K_i$  value in which it interacted with zinc, Thr199, Thr200, Gln92 and Val131 (Figure 5(b)). However, **AAZ** surpassed **2h** binding energy score giving  $-9.12$  Kcal/mol comparing to  $-8.09$  Kcal/mol of **2h** which was translated into a slight difference in their  $K_i$  values.

The following most promising derivative **3c** showed equal sub-nanomolar  $K_i$  values on *hCA II* and *IX* giving 56.4 and 56.9 nM, respectively compared to **AAZ** with  $K_i$  12.0 and 25.0 nM for both isoforms, respectively. Its molecular docking investigation using PDB ID 3HS4 and 3IAI for *hCA II* and *hCA IX*, respectively explained the achieved  $K_i$  values (Figure S11(a,b)). Zinc ion coordination was detected in both isoforms yet, the number of interactions of **3c** with the active site residues were more at *hCA IX* than *hCA II*. This was translated into half the inhibitory activity in case of *hCA IX* compared to almost one-fifth the inhibition in

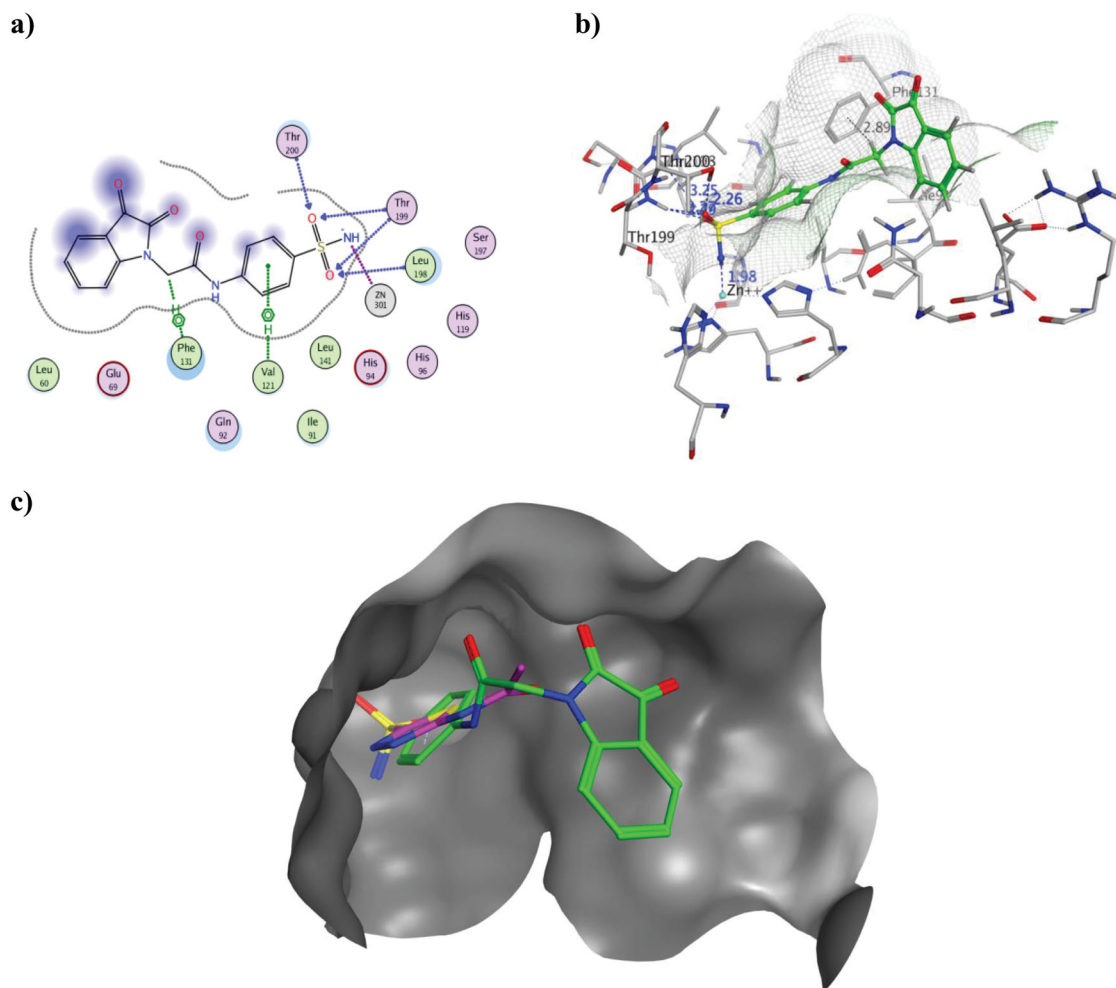


**Figure 4.** Molecular docking data of **2h** on *hCA II* isoform using PDB ID 3HS4 as 2D (a) and 3D (b) presentations showing **2h** as green ball and stick model with the formed H-bonds and arene-H were shown in blue and black dotted lines, respectively with their distance in Å highlighting the interaction site. c) The overlaid 3D presentation of **2h** (green) and **AAZ** (magenta) inside the *hCA II* active site.

case of *hCA II* in comparison to **AAZ**. Furthermore, the superiority of **AAZ** was clarified by its type of interactions with the crucial active site residues of *hCA II* and *hCA IX* (Figure S11(c,d)) together with its favourable binding energy  $-11.85$  and  $-10.98$  Kcal/mol compared to **3c** with  $-8.45$  and  $-9.98$  Kcal/mol for both isoforms, respectively. In contrast, **3c** did not show as promising inhibitory activity on the other two isoforms I and XII which were elucidated by its molecular docking data (Figure S12(a,b)).

### 3.5. 2D-QSAR study

As a useful manipulation of our current and previously achieved *in vitro* *hCA* inhibitory data of benzenesulfonamide derivatives as *hCA* inhibitors, (Figure 6)<sup>29,30</sup>, the tumour associated *hCA IX* and XII data were employed to build two 2D Quantitative Structure-Activity Relationship (2D-QSAR) models given their scaffold similarity, substitution variation and the unified *in vitro* assay method, these QSAR models were used to correlate the achieved inhibitory activity with their structural features for future structural optimisation. The collective biology data showed wide biology spectrum ranges from  $K_i = 14$  to 7336 nM and 8 to 6025 nM for *hCA IX* and *hCAXII*, respectively. Different mathematical forms of the dependent variable were tried such as  $K_i$ ,  $\log K_i$  and  $Pk_i$  where  $\log K_i$  were found to be linear with approximate  $r^2$  value = 0.95 (Figures S13,14). Linear regression method was used for descriptors selection and optimisation by RapidMiner<sup>®</sup> Studio then the model was

generated using Partial Least Square (PLS) method by MOE<sup>®</sup> program. In PLS method, the results of the fit are presented as the root mean square error (RMSE) which is the square root of the MSE function at the chosen descriptors value and the correlation coefficient ( $r^2$ ) which is equal to  $1 - \text{MSE}/\text{YVAR}$  where YVAR is the sample variance of the experimental values<sup>52,53</sup>. The calculated 1D and 2D descriptors by Chemopy<sup>®54</sup> included different constitutional, topological, charge-related, thermodynamic and atom/bond-type descriptors properties of the compounds. An exclusion of descriptors with constant values amongst the training set or equal to zero was done before descriptors selection using the forward linear regression algorithm with leave 10 out validation method of RapidMiner<sup>®</sup> Studio program. The selected descriptors co-linearity of both models was evaluated using correlation matrices to prevent model over-fitting.

#### 3.5.1. 2D-QSAR model of *hCA IX*

For the tumour associated *hCA IX*, the 40 compounds were divided into training  $N=34$  and test  $n=5$  sets and their descriptors were calculated and filtered to 147 after excluding descriptors with fixed values. The selected linear descriptors values of the training set were presented in Table S1. The descriptors governed the activity were found to be the distance and adjacency matrix of the heavy atoms (BCUT\_PEOE-0)<sup>55</sup>, the partial equalisation of orbital electronegativities (PEOE\_VSA-3)<sup>52</sup>, fractional positive polar van der Waals surface area (QVSA\_FPPOS)<sup>56</sup>, partition coefficient of subdivided surface area

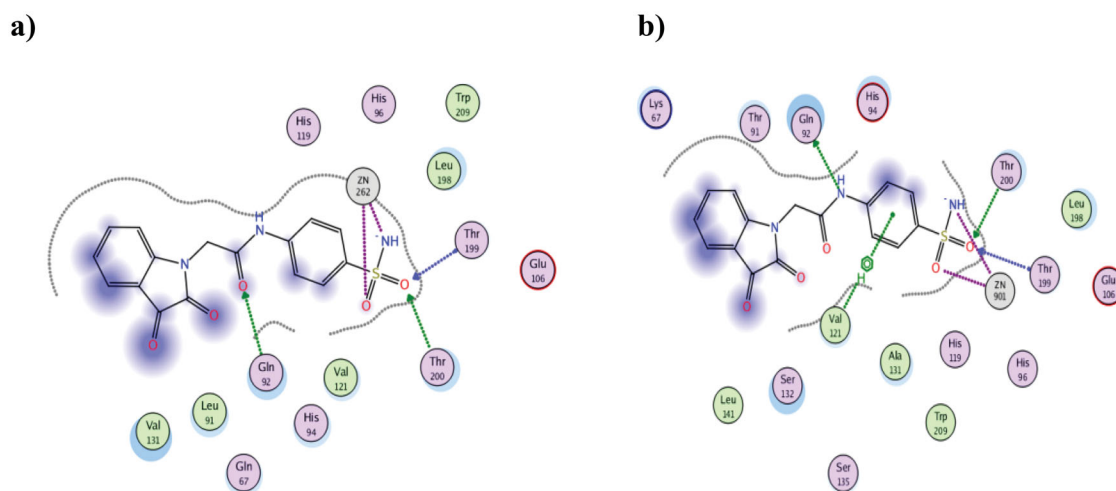


**Figure 5.** The 2D presentation of **2h** molecular docking study interacting with the tumour-associated isoforms *hCA IX* (a) and *hCA XII* (b) using PDB ID 3IAI and 1JD0, respectively.

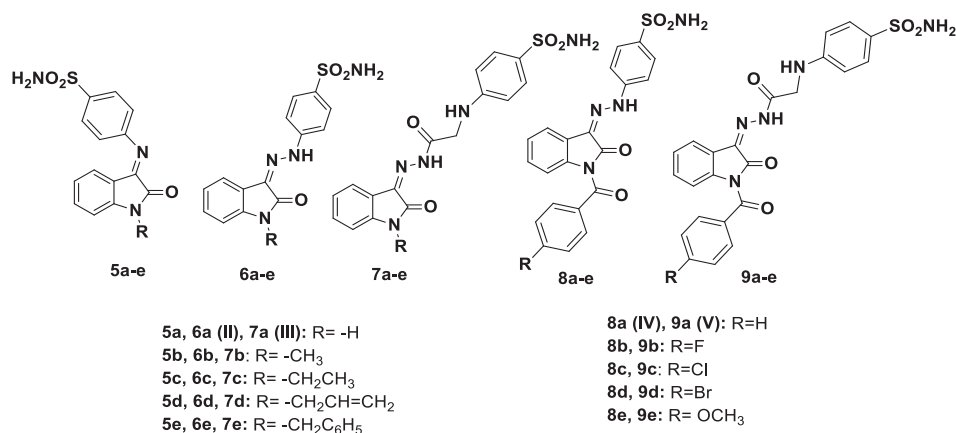


**Figure 6.** Chemical structures of the reported benzenesulfonamide derivatives as *hCA* inhibitors included in the 2D-QSAR training set<sup>29,30</sup>.

(SLogP\_VSA 4)<sup>57</sup> and wiener polarity number (wienerPol)<sup>58</sup> according to the model presented in Equation (1). The generated model showed regression coefficient  $r^2 = 0.862$  and RMSE = 0.269.

$$\begin{aligned} \text{LogK}_i = & 29.73797 + 12.53594 * \text{BCUT}_{\text{PEOE0}} - 0.11013 \\ & * \text{PEOE}_{\text{VSA}-3} - 0.04030 * \text{SlogP}_{\text{VSA}4} \\ & + 0.10445 * \text{wienerPol} - 1.29806 * \text{Q}_{\text{VSA} \text{FPPOS}} \end{aligned} \quad (1)$$

$$\begin{aligned} N = 32, r^2 = 0.862, \text{RMSE} = 0.269, r^2_{(\text{LOO})} \\ = 0.797, r^2_{(\text{validation})} = 0.766, F = 33.039, s^2 = 0.089 \end{aligned}$$

Examining the coefficient values of the independent variables displayed in Equation (1), it revealed that the distance and adjacency of the heavy atoms had the main proportional impact on the dependent inhibitory activity of *hCA IX*. Furthermore, electronegativity and polarity of the compound had appreciable effect on the predicted inhibitory action.

This model was capable of predicting the inhibitory activity of the most potent analogue **7a** amongst all *in-vitro* tested derivatives of benzenesulfonamide with very small difference in log  $K_i$  value of  $-0.11$ . The predicted log  $K_i$  of **7a** was 1.26 ( $K_i = 18.2 \text{ nM}$ ) compared to the actual value 1.146 ( $K_i = 13.9 \text{ nM}$ ).

The generated QSAR model was validated using leave one out (LOO) cross validation method which involved developing a

number of models with one example excluded at a time and externally validated using the test set compounds. The achieved  $r^2_{(\text{LOO})} = 0.797$  with a corresponding RMSE = 0.328 while test set predictive dependent variables showed  $r^2_{(\text{validation})} = 0.766$ . The predictive values of the dependent variables and their corresponding graphical presentation of both LOO and external validation were presented in Table 3 and Figures 7(a,b). As shown in Table 3, the model managed to predict the inhibitory activity of the test set of compounds that were compatible with the actual experimental values with small residuals. Moreover, the obtained Z-score during cross validation remained less than 2.4 suggesting compounds fitting to the generated model with no outliers. Additionally, Fisher-value test (F) and standard deviation ( $s^2$ ) were calculated for the model to confirm its statistical reliability and significance<sup>59</sup>. This model revealed  $F = 33.039$  and  $s^2 = 0.089$  with the higher value of F relative to  $s^2$  was an additional support of the model validation.

### 3.5.2. 2D-QSAR model of *hCA XII*

Similarly, the achieved *hCA XII* inhibitory data was used to construct a 2D-QSAR model to correlate with their physicochemical and topological properties. The compounds were classified into 34 and 6 as training and testing set, respectively where the descriptors selection was done in a similar way to *hCA IX* model complying with the usual linear regression method. The four descriptors governed the activity

**Table 3.** The validation data of *hCAIX* 2D-QSAR model as calculated from LOO method and test set external validation.

Training set (LOO validation)						Test set <sup>a</sup>			
Compd.	log $K_i$	\$PRED	\$Residuals	\$Z-SCORE	\$XPRED	Compd.	log $K_i$	\$PRED	\$ Residuals
7a	1.146	1.261	0.115	0.428	1.298	8a	1.929	1.883	-0.046
6d	1.204	1.171	-0.033	0.123	1.163	8c	2.161	2.102	-0.059
7c	1.204	0.974	-0.23	0.855	0.855	7d	2.418	1.994	-0.424
6a	1.322	1.134	-0.188	0.698	1.036	3e	2.777	2.502	-0.275
5c	1.477	1.483	0.006	0.023	1.488				
7b	1.505	1.653	0.148	0.548	1.702				
3c	1.756	2.388	0.632	2.348	2.463				
2h	1.826	1.546	-0.28	1.041	1.426				
9a	1.833	2.021	0.188	0.702	2.049				
3d	1.935	2.184	0.249	0.927	2.209				
9c	1.968	2.242	0.274	1.016	2.282				
3b	2.09	2.383	0.293	1.088	2.414				
5a	2.13	2.619	0.489	1.815	2.884				
9b	2.155	2.233	0.078	0.289	2.245				
9e	2.217	2.391	0.174	0.646	2.43				
8b	2.236	2.095	-0.141	0.523	2.056				
8e	2.283	2.241	-0.042	0.156	2.232				
9d	2.294	2.249	-0.045	0.169	2.242				
3a	2.334	2.154	-0.18	0.671	2.136				
8d	2.423	2.108	-0.315	1.171	2.011				
3g	2.603	2.509	-0.094	0.352	2.497				
5e	2.752	2.854	0.102	0.378	2.895				
4d	2.759	3.06	0.301	1.12	3.089				
4c	2.816	3.248	0.432	1.609	3.299				
5d	2.828	2.552	-0.276	1.024	2.48				
3f	2.828	2.508	-0.32	1.19	2.473				
4a	2.907	3.015	0.108	0.402	3.027				
5b	2.923	2.825	-0.098	0.365	2.783				
4e	3.498	3.379	-0.119	0.444	3.348				
4b	3.594	3.242	-0.352	1.307	3.199				
4f	3.729	3.358	-0.371	1.379	3.306				
4g	3.865	3.362	-0.503	1.87	3.294				

<sup>a</sup>Compound 7e was excluded from test set as outlier to the model.

were depicted in Equation (2) and Table S2 were the fractional positive polar van der Waals surface area (PEOE\_VSA\_FPPOS)<sup>56</sup>, fractional hydrophobic van der Waals surface area (PEOE\_VSA\_FHYD)<sup>56</sup>, partition coefficient of subdivided surface area (SLogP\_VSA 1)<sup>57</sup> and the total positive partial charge (Q<sub>PC<sup>+</sup></sub>)<sup>56</sup>. The estimated model showed regression coefficient  $r^2 = 0.699$  and RMSE = 0.408.

$$\begin{aligned} \text{Log } K_i = & -8.31628 + 8.98857 * \text{PEOE}_{\text{VSA}}\text{FHYD} - 4.02069 \\ & * \text{PEOE}_{\text{VSA}}\text{FPPOS} + 0.07244 * Q_{\text{PC}^+} + 0.04101 * \text{SlogP}_{\text{VSA}}1 \end{aligned} \quad (2)$$

$$\begin{aligned} N = 33, r^2 = 0.699, \text{RMSE} = 0.408, r^2_{(\text{LOO})} \\ = 0.62, r^2_{(\text{validation})} = 0.841, F = 16.27, s^2 = 0.197 \end{aligned}$$

According to the shown coefficient value of each independent variable in Equation (2), it was suggested that both van der Waals hydrophobic and polar fractional surface area had the main influence on the inhibitory activity of *hCA* XII in direct and inverse proportional, respectively. Similar to *hCA* IX 2D-QSAR model, both fractional positive polar van der Waals surface area and partition coefficient of subdivided surface area had an appreciable effect on the inhibition of *hCA* XII.

The obtained model managed to predict the inhibitory activity of the most potent *hCA*XII inhibitor **2h** amongst the tested analogues with difference of 0.051. The model suggested a log  $K_i$  of 0.954 ( $K_i = 8.99$  nM) compared to the actual log  $K_i$  of 0.903 ( $K_i = 7.91$  nM).

Resembling the *hCAIX* inhibitors 2D-QSAR model validation parameters, the predicative log  $K_i$  values were presented in Table 4. This model displayed  $r^2_{(\text{LOO})} = 0.62$  with RMSE = 0.46 however, its external validation using the test set revealed more

promising  $r^2_{(\text{validation})} = 0.841$  (Figure 8(a,b)) accompanied with  $F = 16.27$  and  $s^2 = 0.197$ .

Considering the formerly mentioned internal and external validation and statistical analysis of the calculated descriptors of both *hCA* IX and XII 2D-QSAR models, it was concluded that they showed sufficient predictive capability of the inhibitory activity with minimal error.

#### 4. Conclusion

From our current study we can conclude that isatin *N*-phenylacetamide based sulphonamides could be considered as promising scaffold for future research to develop potent and selective carbonic anhydrase inhibitors along with anti-proliferative activity. It was observed that 2,3-dioxindole **2h**, hydrazinyl benzenesulfonamides **3c** and **3d** were relatively the most potent ones. Derivative **2h** showed promising potency against all tested isoforms with the best inhibitory activity towards *hCA*I and *hCA* II ( $K_i = 45.10$  and  $5.87$  nM, respectively) more than that of acetazolamide (AZZ) (250 and 12 nM, respectively). Moreover, compounds **3c** and **3d** showed good cytotoxicity where compound **3c** revealed a promising selectivity towards human lung adenocarcinoma A549 (SI = 16.94). Docking simulation of the most active ones **2h** and **3c** predicted their binding pattern and binding affinity to the *hCA* II, IV, IX and XII active sites and rationalising their selectivity based on their docking binding patterns and scores. Furthermore, 2D-QSAR developed models using training set of the published data of our previous work of benzenesulfonamide derivatives as *hCA* IX and XII inhibitors showed sufficient predictive capability of the inhibitory activity with minimal error.

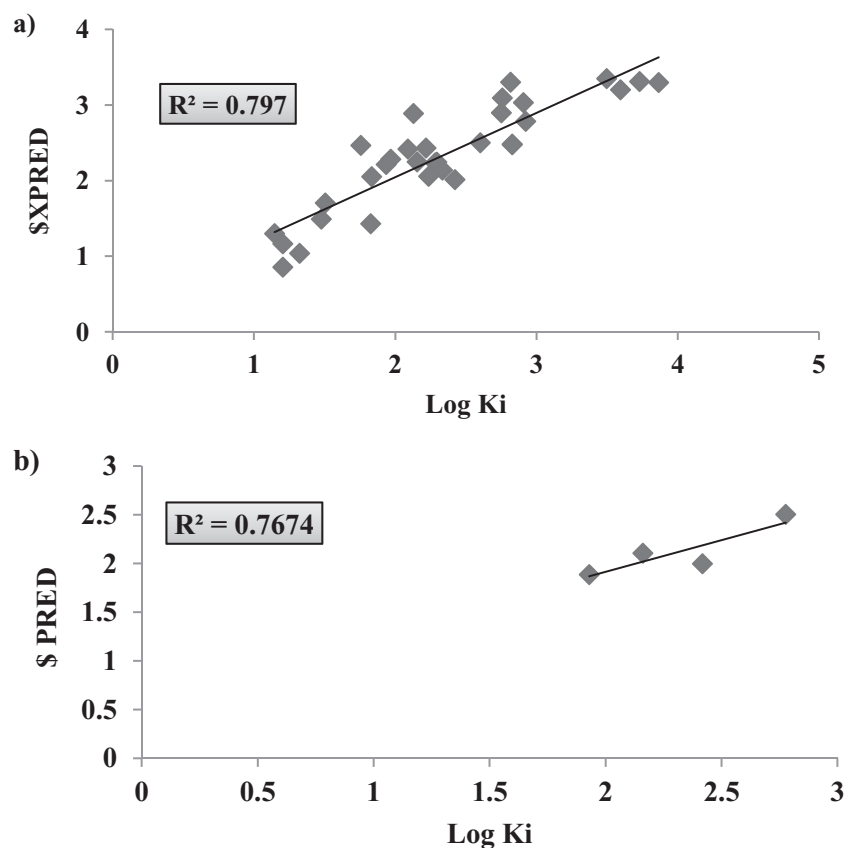


**Figure 7.** Graphical presentation between the experimental and predicative log  $K_i$  of *hCAXII* training set (LOO) validation (a) and test set (b) where the corresponding squared linear coefficient  $r^2$  were displayed.

**Table 4.** The validation data of *hCAXII* 2D-QSAR model as calculated from LOO method and test set external validation.

Training set (LOO validation)						Test set			
Compd.	Log $K_i$	\$PRED	\$RES	\$Z-SCORE	\$XPRED	Compd.	Log $K_i$	\$PRED	\$ Residuals
2h	0.903	0.954	-0.051	0.124	0.997	5b	1.531	1.035	0.496
9a	1.342	1.906	-0.563	1.378	1.968	5d	1.851	1.311	0.54
9e	1.342	2.065	-0.722	1.766	2.147	8d	1.949	2.181	-0.231
8e	1.491	2.16	-0.669	1.636	2.193	6c	2.666	2.183	0.482
8a	1.519	2.015	-0.497	1.214	2.038	4f	2.877	2.999	-0.122
8c	1.623	2.121	-0.498	1.217	2.145	4c	3.359	3.053	0.306
5e	1.623	1.546	0.077	0.188	1.511				
8b	1.681	1.771	-0.09	0.22	1.777				
6b	1.756	2.077	-0.321	0.785	2.125				
7b	1.792	1.825	-0.032	0.079	1.826				
5c	1.881	1.163	0.718	1.756	0.958				
9b	1.898	1.698	0.2	0.489	1.663				
5a	1.919	1.539	0.38	0.93	1.457				
9c	1.934	2.015	-0.081	0.197	2.023				
7c	1.964	1.941	0.023	0.056	1.94				
9d	2.114	2.078	0.036	0.089	2.075				
7d	2.283	2.081	0.202	0.494	2.067				
6a	2.439	2.621	-0.182	0.445	2.685				
7e	2.452	2.307	0.144	0.353	2.287				
3b	2.676	3.095	-0.42	1.026	3.135				
3e	2.777	3.127	-0.35	0.855	3.159				
7a	2.78	2.357	0.424	1.036	2.275				
3c	2.787	3.145	-0.359	0.877	3.184				
3d	2.851	3.091	-0.24	0.587	3.114				
3g	2.884	3.145	-0.261	0.639	3.174				
4a	2.884	2.904	-0.02	0.05	2.907				
4g	2.926	3.053	-0.127	0.31	3.067				
6d	2.98	2.314	0.666	1.63	2.211				
4e	3.182	3.041	0.142	0.347	3.021				
3f	3.518	3.095	0.423	1.033	3.056				
3a	3.562	3.006	0.557	1.361	2.96				
4b	3.703	2.999	0.704	1.721	2.918				
4d	3.78	2.995	0.785	1.92	2.907				

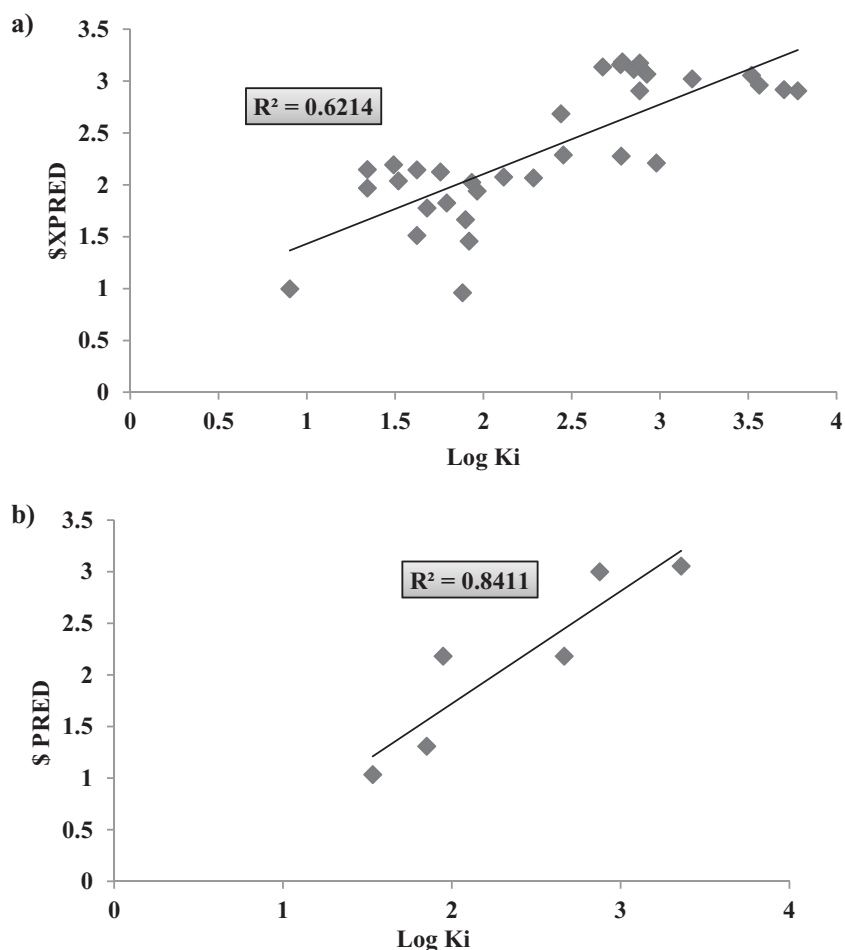


**Figure 8.** Graphical presentation between the experimental and predicative log  $K_i$  of hCAXII training set (LOO) validation (a) and test set (b) where the corresponding squared linear coefficient  $r^2$  were displayed.

### Disclosure statement

No potential conflict of interest was reported by all authors. CT Supuran is Editor-in-Chief of the Journal of Enzyme Inhibition and Medicinal Chemistry. He was not involved in the assessment, peer review, or decision-making process of this paper. The authors have no relevant affiliations of financial involvement with any organisation or entity with a financial interest in or financial conflict with the subject matter or materials discussed in the manuscript. This includes employment, consultancies, honoraria, stock ownership or options, expert testimony, grants or patents received or pending, or royalties.

### Funding

The carbonic anhydrase inhibition assay in this research was financed by the Italian Ministry for Education and Science (MIUR), grant PRIN: rot. 2017XYBP2R and by Ente Cassa di Risparmio di Firenze (ECRF), grant CRF2020.1395 to CTS.

### ORCID

Riham F. George  <http://orcid.org/0000-0002-2493-1315>

Claudiu T. Supuran  <http://orcid.org/0000-0003-4262-0323>

### References

- Supuran CT. Structure and function of carbonic anhydrases. *Biochem J* 2016;473:2023–32.
- Boone CD, Pinard M, McKenna R, Silverman D. Catalytic mechanism of  $\alpha$ -class carbonic anhydrases: CO<sub>2</sub> hydration and proton transfer. *Subcell Biochem* 2014;75:31–52.
- McKenna R, Supuran CT. Carbonic anhydrase inhibitors drug design. *Subcell Biochem* 2014;75:291–323.
- Supuran CT. Structure-based drug discovery of carbonic anhydrase inhibitors. *J Enzyme Inhib Med Chem* 2012;27: 759–72.
- Luca LD, Mancuso F, Ferro S, et al. Inhibitory effects and structural insights for a novel series of coumarin-based compounds that selectively target human CA IX and CA XII carbonic anhydrases. *Eur J Med Chem* 2018;143: 276–82.
- Neri D, Supuran CT. Interfering with pH regulation in tumours as a therapeutic strategy. *Nat Rev Drug Discov* 2011;10:767–77.
- Awadallah FM, El-Waei TA, Hanna MM, et al. Synthesis, carbonic anhydrase inhibition and cytotoxic activity of novel chromone-based sulfonamide derivatives. *Eur J Med Chem* 2015;96:425–35.
- Awadallah FM, Bua S, Mahmoud WR, et al. Inhibition studies on a panel of human carbonic anhydrases with N1-

- substituted secondary sulfonamides incorporating thiazolone or imidazolone-indole tails. *J Enzyme Inhib Med Chem* 2018;33:629–38.
9. Ghorab MM, Alsaïd MS, Soliman AM, Al-Mishari AA. Benzo[g]quinazolin-based scaffold derivatives as dual EGFR/HER2 inhibitors. *J Enzyme Inhib Med Chem* 2018;33:67–73.
  10. Ghorab MM, Alsaïd MS, Soliman AM, Ragab FA. VEGFR-2 inhibitors and apoptosis inducers: synthesis and molecular design of new benzo[g]quinazolin bearing benzenesulfonamide moiety. *J Enzyme Inhib Med Chem* 2017;32:893–907.
  11. Mboge MY, McKenna R, Frost SC. Advances in anti-cancer drug development targeting carbonic anhydrase IX and XII. *Top Anti-Cancer Res* 2015;5:3–42.
  12. Supuran CT. Carbonic anhydrase inhibitors as emerging agents for the treatment and imaging of hypoxic tumors. *Expert Opin Investig Drugs* 2018;27:963–70.
  13. Krasavin M, Korsakov M, Dorogov M, et al. Probing the 'bipolar' nature of the carbonic anhydrase active site: aromatic sulfonamides containing 1,3-oxazol-5-yl moiety as picomolar inhibitors of cytosolic CA I and CA II isoforms. *Eur J Med Chem* 2015;101:334–3478.
  14. Ibrahim HS, Allam HA, Mahmoud WR, et al. Dual-tail arylsulfone-based benzenesulfonamides differently match the hydrophobic and hydrophilic halves of human carbonic anhydrases active sites: Selective inhibitors for the tumor-associated hCA IX isoform. *Eur J Med Chem* 2018;152:1–9.
  15. Chiamonte N, Romanelli MN, Teodori E, Supuran CT. Amino acids as building blocks for carbonic anhydrase inhibitors. *Metabolites* 2018;8:36–57.
  16. Supuran CT. Diuretics: from classical carbonic anhydrase inhibitors to novel applications of the sulfonamides. *Curr Pharm Des* 2008;14:641–8.
  17. Borrás J, Scozzafava A, Menabuoni L, et al. Carbonic anhydrase inhibitors: synthesis of water-soluble, topically effective intraocular pressure lowering aromatic/heterocyclic sulfonamides containing 8-quinoline-sulfonyl moieties: is the tail more important than the ring? *Bioorg Med Chem* 1999;7:2397–406.
  18. Supuran CT. Acetazolamide for the treatment of idiopathic intracranial hypertension. *Expert Rev Neurother* 2015;15:851–6.
  19. Ghorab MM, Soliman AM, Alsaïd MS, Askar AA. Synthesis, antimicrobial activity and docking study of some novel 4-(4,4-dimethyl-2,6-dioxocyclohexylidene) methylamino derivatives carrying biologically active sulfonamide moiety. *Arab J Chem* 2020;13:545–56.
  20. Borne RF, Peden RL, Waters I, et al. Anti-inflammatory activity of para-substituted N-benzenesulfonyl derivatives of anthranilic acid. *J Pharm Sci* 1974;63:615–7.
  21. Soliman AM, Karam HM, Mekki MH, Ghorab MM. Antioxidant activity of novel quinazolinones bearing sulfonamide: potential radiomodulatory effects on liver tissues via NF- $\kappa$ B/PON1 pathway. *Eur J Med Chem* 2020;197:112333.
  22. Soliman AM, Alqahtani AS, Ghorab M. Novel sulphonamide benzoquinazolinones as dual EGFR/HER2 inhibitors, apoptosis inducers and radiosensitizers. *J Enzyme Inhib Med Chem* 2019;34:1030–40.
  23. Ghorab MM, Alsaïd MS, El-Gaby MS, et al. Biological evaluation of some new N-(2,6-dimethoxypyrimidinyl) thioureido benzenesulfonamide derivatives as potential antimicrobial and anticancer agents. *Eur J Med Chem* 2016;124:299–310.
  24. Ghorab MM, Ragab FA, Heiba HI, Soliman AM. Anticancer and radiosensitizing evaluation of some new sulfonamide derivatives bearing pyridone, thiophene, and hydrazone moieties. *Res Chem Intermed* 2017;43:4657–81.
  25. Chow LQ, Eckhardt SG. Sunitinib: from rational design to clinical efficacy. *J Clin Oncol* 2007;25:884–96.
  26. Abo-Ashour MF, Eldehna WM, Nocentini A, et al. Novel hydrazido benzenesulfonamides-isatin conjugates: Synthesis, carbonic anhydrase inhibitory activity and molecular modeling studies. *Eur J Med Chem* 2018;157:28–36.
  27. Abo-Ashour MF, Eldehna WM, Nocentini A, et al. 3-Hydrazinoisatin-based benzenesulfonamides as novel carbonic anhydrase inhibitors endowed with anticancer activity: Synthesis, in vitro biological evaluation and in silico insights. *Eur J Med Chem* 2019;184:111768.
  28. Eldehna WM, Abo-Ashour MF, Nocentini A, et al. Enhancement of the tail hydrophobic interactions within the carbonic anhydrase IX active site via structural extension: Design and synthesis of novel N-substituted isatins-SLC-0111 hybrids as carbonic anhydrase inhibitors and antitumor agents. *Eur J Med Chem* 2019;162:147–60.
  29. George RF, Said MF, Bua S, Supuran CT. Synthesis and selective inhibitory effects of some 2-oxindole benzenesulfonamide conjugates on human carbonic anhydrase isoforms CA I, CA II, CA IX and CAXII. *Bioorg Chem* 2020;95:103514.
  30. George RF, Bua S, Supuran CT, Awadallah FM. Synthesis of some N-aryl-2-oxindole benzenesulfonamide conjugates with carbonic anhydrase inhibitory activity. *Bioorg Chem* 2020;96:103635.
  31. Kumar R, Kaur M, Bahia MS, Silakari O. Synthesis, cytotoxic study and docking based multidrug resistance modulator potential analysis of 2-(9-oxoacridin-10(9H)-yl)-N-phenyl acetamides. *Eur J Med Chem* 2014;80:83–91.
  32. Monforte AM, Ferro S, Luca LD, et al. Design and synthesis of N<sup>1</sup>-aryl-benzimidazoles 2-substituted as novel HIV-1 non-nucleoside reverse transcriptase inhibitors. *Bioorg Med Chem* 2014;22:1459–67.
  33. Wang Y, Chan FY, Sun N, Lui HK, et al. Structure-based Design, Synthesis, and Biological Evaluation of Isatin Derivatives as Potential Glycosyltransferase Inhibitors. *Chem Biol Drug Des* 2014;84:685–96.
  34. Akgul O, Tarikogullari AH, Kose FA, Ballar P. Synthesis and cytotoxic activity of some 2-(2,3-dioxo-2,3-dihydro-1H-indol-1-yl)acetamide derivatives. *Turkish J Chem* 2013;37:204–12.
  35. Firozpour L, Gao L, Moghimi S, et al. Efficient synthesis, biological evaluation, and docking study of isatin based derivatives as caspase inhibitors. *J Enzyme Inhib Med Chem* 2020;35:1674–84.
  36. Soliman R. Preparation and antidiabetic activity of some sulfonamide derivatives of 3,5-disubstituted pyrazoles. *J Med Chem* 1979;22:321–5.
  37. Wani TV, Bua S, Khude PS, et al. Evaluation of sulfonamide derivatives acting as inhibitors of human carbonic anhydrase isoforms I, II and Mycobacterium tuberculosis  $\beta$ -class enzyme Rv3273. *J Enzyme Inhib Med Chem* 2018;33:962–71.
  38. Khalifah RG. The carbon dioxide hydration activity of carbonic anhydrase. I. Stopflow kinetic studies on the native human isoenzymes B and C. *J Biol Chem* 1971;246:2561–73.
  39. Nocentini A, Trallori E, Singh S, et al. 4-Hydroxy-3-nitro-5-ureido-benzenesulfonamides selectively target the tumor-associated carbonic anhydrase isoforms IX and XII showing hypoxia-enhanced antiproliferative profiles. *J Med Chem* 2018;61:10860–74.



40. Entezari Heravi Y, Bua S, Nocentini A, et al. Inhibition of *Malassezia globosa* carbonic anhydrase with phenols. *Bioorg Med Chem* 2017;25:2577–82.
41. Nocentini A, Carta F, Tanc M, et al. Deciphering the mechanism of human carbonic anhydrases inhibition with sulfocoumarins: computational and experimental studies. *Chemistry* 2018;24:7840–4.
42. Nocentini A, Lucidi A, Perut F, et al.  $\alpha,\gamma$ -Diketocarboxylic acids and their esters act as carbonic anhydrase IX and XII selective inhibitors. *ACS Med Chem Lett* 2019;10:661–5.
43. Skehan P, Storeng R, Scudiero D, et al. 82(13);, New colorimetric cytotoxicity assay for anticancer-drug screening. *J Natl Cancer Inst* 1990;82:1107–12.
44. Allam RM, Al-Abd AM, Khedr A, et al. Abdel-Naim AB. Fingolimod interrupts the cross talk between estrogen metabolism and sphingolipid metabolism within prostate cancer cells. *Toxicol Lett* 2018;291:77–85.
45. Eldehna WM, Fares M, Ceruso M, et al. Amido/ureidosubstituted benzenesulfonamides-isatin conjugates as low nanomolar/subnanomolar inhibitors of the tumor-associated carbonic anhydrase isoform XII. *Eur J Med Chem* 2016;110:259–66.
46. Smirnov AS, Nikolaev DN, Gurzhiy VV, Smirnov SN, Suslonov VS, et al. Conformational stabilization of isatin Schiff bases-biologically active chemical probes. *RSC Adv* 2017;7:10070–3.
47. Chia SK, Wykoff CC, Watson PH, et al. Prognostic significance of a novel hypoxia-regulated marker, carbonic anhydrase IX, in invasive breast carcinoma. *J Clin Oncol* 2001;19:3660–8.
48. Ilie M, Mazure NM, Hofman V, et al. High levels of carbonic anhydrase IX in tumour tissue and plasma are biomarkers of poor prognostic in patients with non-small cell lung cancer. *Br J Cancer* 2010;102:1627–35.
49. Available from: <https://www.rcsb.org>
50. Kanamori K, Roberts JD. Nitrogen-15 nuclear magnetic resonance study of benzenesulfonamide and cyanate binding to carbonic anhydrase. *Biochemistry* 1983;22:2658–64.
51. Briganti F, Mangani S, Orioli P, et al. Carbonic anhydrase activators: X-ray crystallographic and spectroscopic investigations for the interaction of isozymes I and II with histamine. *Biochemistry* 1997;36:10384–92.
52. Helland IS. On the structure of partial least squares regression. *Comm Statist B, Simulation Comput* 1988;17:581–607.
53. Geladi P, Kowalski R. Partial least squares regression: a tutorial. *Analytica Chimica Acta* 1986;185:1–17.
54. Chemopy Descriptor Calculator. [http://www.scbdd.com/chemopy\\_desc/index/](http://www.scbdd.com/chemopy_desc/index/) (6/10/2021).
55. Pearlman RS, Smith KM. Novel software tools for chemical diversity. *Persp Drug Disc Des* 1998;9:339–53.
56. Gasteiger J, Marsili M. Iterative partial equalization of orbital electronegativity - a rapid access to atomic charges. *Tetrahedron* 1980;36:3219–28.
57. Wildman SA, Crippen GM. Prediction of physiochemical parameters by atomic contributions. *J Chem Inf Comput Sci* 1999;39:868–73.
58. Balaban AT. Five new topological indices for the branching of tree-like graphs. *Theoretica Chimica Acta* 1979;53:355–75.
59. Gramatica P, On the Development and Validation of QSAR Models. In: *Computational toxicology: Volume II, Methods in molecular biology*. Reisfeld MA. Springer Science + Business Media, LLC; 2013, p. 499–526.